Jimma University

Jimma Institute of Technology

Faculty of Mechanical Engineering

Design Optimization through CFD Simulation and Experimental Validation of a Finned Phase Change Material (PCM) Thermal Energy Storage for Solar Cooking Application

(A Case Study of Jimma)

By: Abraha Kahsay Kiros

A Thesis Submitted to School of Graduate Studies of Jimma University, in Partial Fulfilment of the Requirements for the Degree of Master of Science in Mechanical Engineering (Thermal Systems Engineering Stream)

June, 2020

Jimma, Ethiopia

Design Optimization through CFD Simulation and Experimental validation of a Finned Phase Change Material (PCM) Thermal Energy Storage for Solar Cooking Application

(A Case Study of Jimma)

By: Abraha Kahsay Kiros

A Thesis Submitted to School of Graduate Studies of Jimma University, in Partial Fulfilment of the Requirements for the Degree of Master of Science in Mechanical Engineering (Thermal Systems Engineering Stream)

Main Advisor: Balewgize Amare Zeru (Asst. Prof.)

Co-advisor: Debela Geneti (MSc.)

June, 2020

Jimma, Ethiopia

Declaration

I, the under signed, declare that this research entitled by *"Design Optimization through CFD Simulation and Experimental Validation of a Finned Phase Change Material (PCM) Thermal Energy Storage for Solar Cooking Application (a case study of Jimma)* is my original work, and has not been presented by any other person for an award of a degree in this or any other University, and all sources of materials used for the thesis have been duly acknowledged.

Abraha Kahsay   21/06/2020

Name   Signature   Date

This thesis is approved by:

Balewgize Amare (Asst. Prof.)   29/06/2020

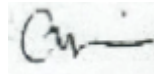**Main Advisor**   Signature   Date

Debela Geneti (MSc.)   29/06/2020

Co-Advisor   Signature   Date

Getachew Shunki Tibba (Dr.-Ing.)   29/06/2020

External Examiner   Signature   Date

Nebiyu Bogale (Asst. Prof.)   29/06/2020

Internal Examiner   Signature   Date

Fikadu Kifle (MSc.)   29/06/2020

Chair Person   Signature   Date

Abstract

The interest of exploiting solar energy for electrification and other household applications such as heating and cooking is increasing due to the reason that they are clean and ecofriendly. In doing so, energy storage mediums are integrated to maintain the energy demand with the intermittent nature of solar energy. Phase change materials (PCMs) has shown a great energy storage use in solar thermal applications despite their low thermal conductivity property which makes low heat transfer during charge/discharge or energy store/release process. Studies show embedding extended surfaces (fins) in the PCM is easier and economical among the different heat transfer enhancement methods. But there are limited works on the problem of increasing geometric parameters of fins, as it replaces the mass of the PCM which results in reduced latent heat storage.

This work intends to study and optimize the heat transfer rate and latent heat storage of a solar cooking with finned heat storage system. The study was started by collecting the energy demand for household cooking and solar irradiance assessment of the study site. Following this bench mark, a PCM vessel and parabolic trough solar collector were designed. Numerical simulations using CFD tool ANSYS 16.0 and experiments has been conducted to investigate the effect of fin length and thickness on the performance of the system. Design optimization was made using response surface methodology with central composite design for design points.

Hitec salt or molten salt with 53% KNO_3, 6% $NaNO_3$ and 41% $NaNO_2$ by composition (with 142 °C melting temperature, 110 kJ/kg heat of fusion) is selected as suitable PCM material for the application. The findings show that increasing fin length show better heat transfer rate than increasing fin thickness. The thicker and longer fin with dimensions of 1.5 and 140 mm respectively, gave 65.97% faster rate than the system without fin. In the optimization process it was found that the fin with 0.8 mm thickness and 140 mm length gives optimized design for the heat transfer rate and energy storage capacity. The optimized design takes 10.21 hr. for complete solidification process and can release 2237.91kJ heat.

Key words: Phase change materials (PCM), solar cook, Thermal energy storage, optimization, Fin, heat transfer rate, heat storage capacity, CFD

Acknowledgment

First of all, my special thanks goes to God who gave me the patience, love, courage and strength during my study.

I would like to express my deepest gratitude for my advisor, Balewgize Amare Zeru (Asst. Prof.) for his positive attitude, continuous support, encouragement and excellent supervision. He has been source of inspiration and it was great experience to work with him, I would like also to thank my co-advisor Mr. Debela Geneti (MSc.) for his guidance and encouragement.

My next gratitude goes to Mr. Mitiku Seboka and all the laboratory staff members at Faculty of Mechanical Engineering who were by my side during the lab work.

Finally, I am grateful to my family, friends, staff members and all the countless who made my life joyful and meaningful.

1 Table of Contents

Nomenclature, Abbreviations and Symbols

Nomenclature

K	thermal conductivity (W/m.K)
h	heat transfer coefficient (W/(m^2.K))
Cp	specific heat capacity (J/kg.K)
h_{fg}	heat of fusion (J/kg)
Q	heat quantity (J)
$\dot{Q}$	rate of heat transfer (W)
m	mass (kg)
V	volume (m^3)
$\dot{v}$	volume flow rate (m^3/s)
T	temperature (K)
A_c	area of collector
A_r	area of absorber

Abbreviations

TES	Thermal Energy Storage
SHS	Sensible Heat Storage
LHS	Latent Heat Storage
TCS	Thermo-Chemical Storage
PCM	Phase Change Material
HTF	Heat Transfer Fluid
LHTES	Latent Heat Thermal Energy Storage
GIS	Geographic Information System
CFD	Computational Fluid Dynamics
ANSYS	ANalysis System
RSM	Response Surface Methodology
CCD	Central Composite Design

PTSC Parabolic Trough Solar Collector

ETSC Evacuated Tube Solar Collector

Greek letters

ω_s Sunset hour angle (°)

δ sun declination angle (°)

ϕ Altitude angle (°)

ϕ_r rim angle (°)

η efficiency (%)

σ Stefan-*Boltzmann constant* (5.67×10^{-8} W m^{-2} K^{-4})

ρ density (kg m^{-3})

π pi

μ dynamic viscosity

β liquid fraction

List of Tables

List of Figures

1 Introduction

1.1 Background of the study

In Ethiopia, Eighty-three percent of the population resides in rural areas, largely relying on traditional biomass energy sources for cooking and heating. Biomass accounts for 91% of energy consumed. Petroleum supplies about 7% of total primary energy and electricity accounts for only 2% of total energy use [1]. The primary energy demand of the large percentage of the population is therefore for cooking. Women and children are prone to collecting dry biomass that may last for a day which is time consuming and tedious. This affects the educational background of the young population and the environment. In addition, there will be much generation of smoke as a result of burning wood or dung. Particles and toxic compounds are contained in the fumes, which generates damages and illnesses on eyes and on the respiratory track.

Although fuel oils are also widely used energy sources, nowadays the energy trend is shifting to renewable sources due to cost, unsustainability and environmental problems of the fuel oils. This challenge has created an interest in exploiting solar energy which is one form of renewable energy source which is versatile and promising. It has been applicable in electrification, drying crops, cooking and heating, and refrigeration and air conditioning systems.

Ethiopia receives a solar irradiation of 5000 – 7000 Wh/m² according to region and season and thus has great potential for the use of solar energy. The average solar radiation is more or less uniform, around 5.2 kWh/m^2/day. The values vary seasonally, from 4.55-5.55 kWh/m^2/day and with a location from 4.25 kWh/m^2/day in the extreme western lowlands to 6.25 kWh/m^2/day in Adigrat area, Northern Ethiopia [2]. It can also be observed that there is high solar radiation cover in the north-western and south-eastern regions of the country as shown in figure1.
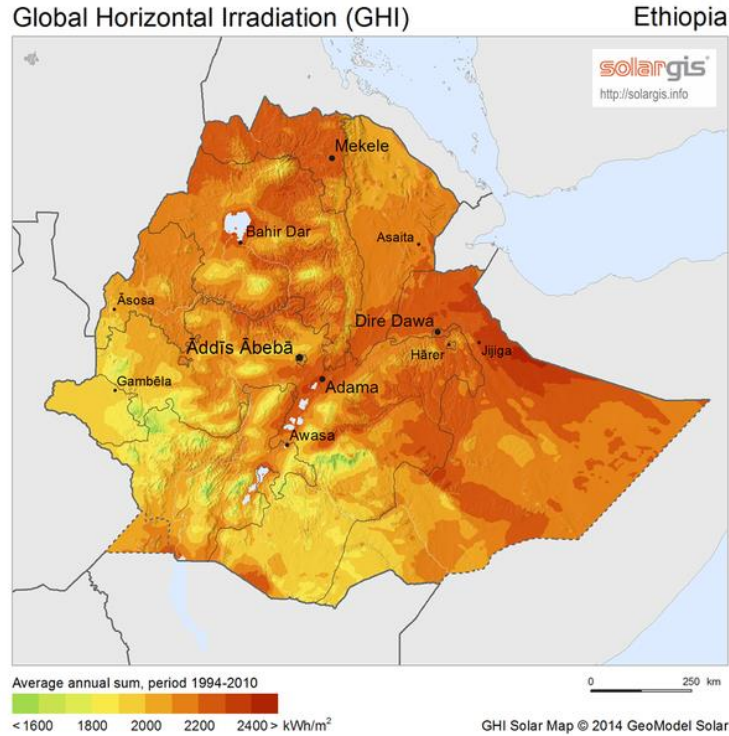
Figure 1. Ethiopian solar GIS map [3]

The nature of solar energy is intermittent due to fluctuating weather conditions and day/night variations. This fluctuation causes problem in energy demand for continuous use. As a solution, thermal energy storages (TES) which store heat, play a significant role in harnessing solar energy for off conditions and maintaining variations during cloudy days.

Thermal energy can be stored while there is excess energy and can be used for later when it is required. Thermal energy storages can be classified in three forms.

- Sensible heat storage (SHS),
- Latent heat storage (LHS) and
- Thermo-chemical storage (TCS).

In sensible thermal energy storage system, the storage material gets temperature change when it is heated and energy is stored in the form of internal energy. The amount of stored thermal energy (Q) can be easily estimated as the product of mass m, specific heat capacity and temperature uplift ΔT of the material, as in equation (1):

$$Q = \int_{T_1}^{T_2} m.C_p.dT \qquad (1)$$

In latent heat storage, thermal energy is stored during phase change of materials. For instance during solid-liquid phase change of a material, energy is stored during melting and released during solidification. Figure2 shows how phase change materials charge/discharge energy by heating and cooling. The material used in latent heat energy storage is called phase change material (PCM).
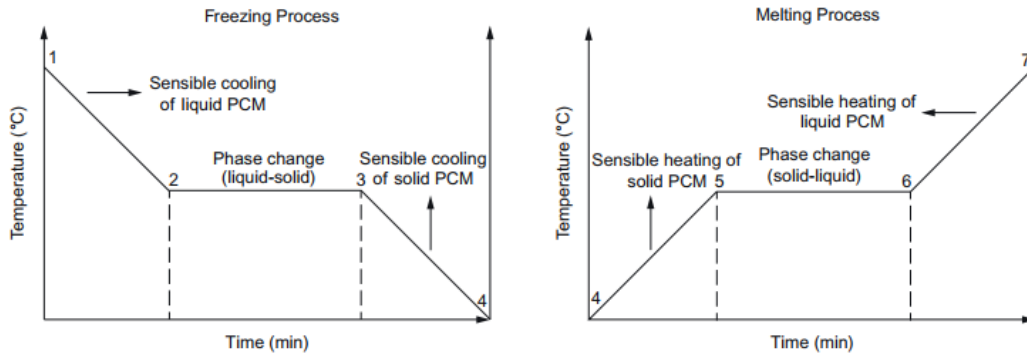
Figure 2. Energy storage and release process of a PCM. [4]

The amount of stored energy (Q) is the sum of the sensible heat stored in both phases and the latent heat involved in phase-transformation, which is the main portion of energy storage.

$$Q = \int_{T_1}^{T_m} m.C_{p,1}.dT + m.f.\Delta H_m + \int_{T_m}^{T_2} m.C_{p,2}.dT \qquad (2)$$

Where ΔH_m- is heat of melting per unit mass (J/kg), f – is melt fraction and T_m- is the phase change temperature.

In the third type of energy storage (thermo-chemical storage), thermal energy is stored in similar way as LHS. The major difference is that thermal energy is mainly stored as the enthalpy change in thermo-chemical reaction, instead of phase-transformation process.

3

For a specific requirement of thermal energy, sensible heat storage requires a larger vessel as compared with latent heat and thermochemical storages. Thermochemical storage on the other hand, is associated with high energy storage density but still at pre-matured stage in terms of research and development. Among the three thermal energy storage methods, latent heat energy storage is the most promising and attractive due to its compactness and ability to store energy at nearly constant temperature corresponding to the phase transition temperature of the material [5]. However, the main disadvantage of LHS is its low thermal conductivity, which mostly fall in the range of 0.2 W/(m·K) to 0.7 W/(m·K) which needs effective heat transfer enhancement technologies.

In heat transfer applications it is common to have combined heat transfer modes like both conduction and convection. For this reason, in heat exchangers which may contain two fluids or fluid/solid interaction, the heat transfer can be expressed as:

$$Q = UA_s\Delta T \tag{3}$$

Where U is the overall heat transfer coefficient, A_s is the surface area and ΔT represents the temperature difference between the two mediums for instance (PCM and HTF).

It can be seen that the three parameters (U, A_s and ΔT) are directly proportional to the heat transfer rate and increasing one or more of these variables will enhance the heat transfer rate (Q). Therefore, the problem of low thermal conductivity in PCMs which affects the conductive heat transfer can be improved by choosing from these options.

PCMs can be integrated with solar cooking in different ways. There are solar cookers which use the solar radiation directly and on the other hand there are solar collectors which involve heat transfer fluid for indirect (indoor cooking) application.

Solar radiation can be used directly to charge the storage medium and then the stored energy will be used for cooking. Box-type cookers, the ones with flat plate solar collectors (FPSC) with the solar absorbers enclosed in a glazed box can be mentioned in this category. Concentrating solar collectors like dish collector can also be used for direct use if there is no involvement of heat transfer fluid (figure3).
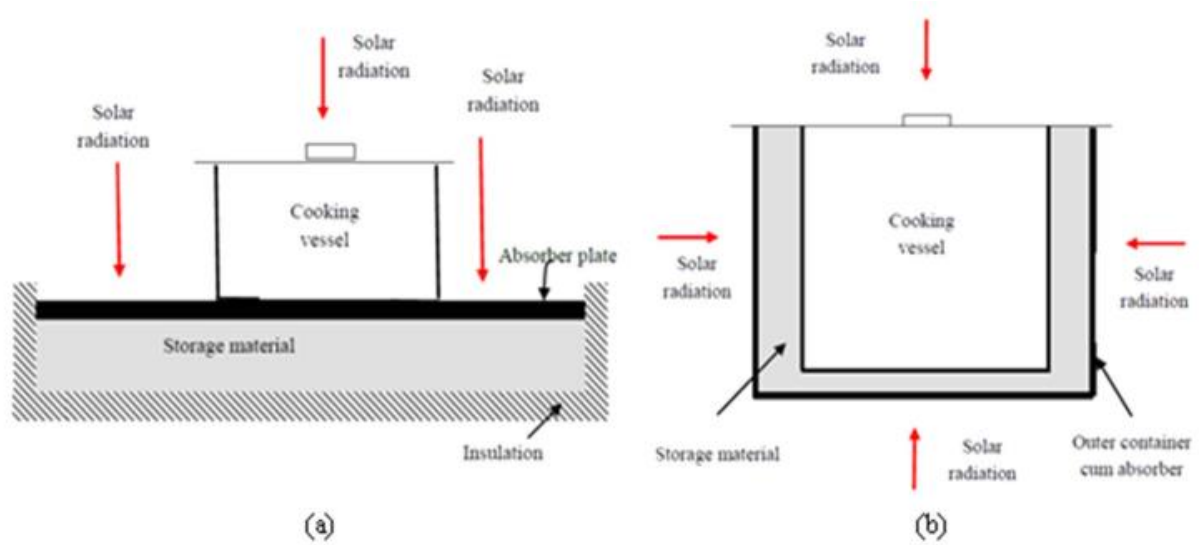
Figure 3. Direct solar cooking process without HTF. [6]

In higher operating temperatures with the use of concentrating solar collectors (CSC) and to smaller degree of Evacuated tube solar collectors (ETSC), there will be the involvement of heat transfer fluid (HTF). In these systems, heat is transported from the solar absorber to HTF that charges the storage medium and then the storage medium releases the heat for cooking load (figure4). This system is good for indoor cooking that reduce human exposure to solar radiation.
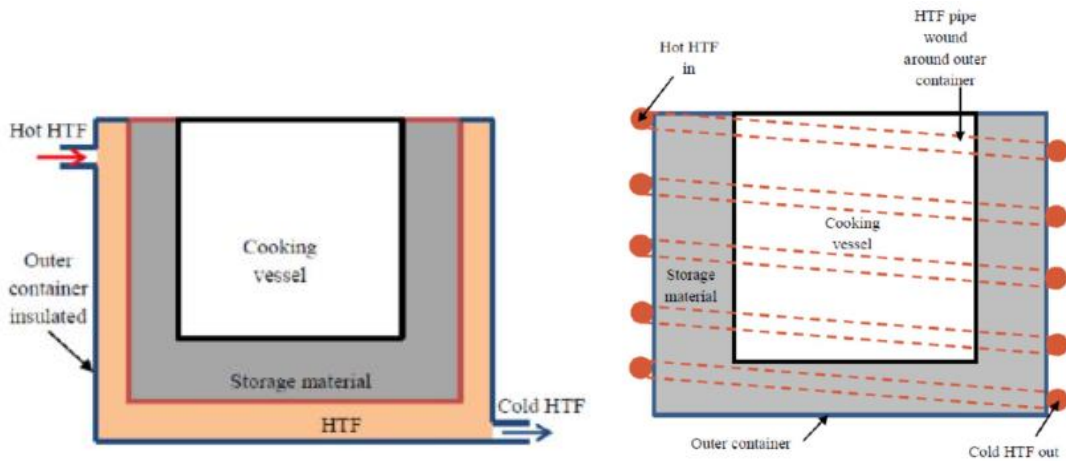
Figure 4. Solar cooking process that involve HTF [6]

1.2   Statement of the problem

Phase change materials (PCM) are a typical energy storage mediums which provide the advantage of small volume and high energy storage capacity in thermal applications. Due to this reason, they have a great potential in exploiting solar energy for cooking and other heating applications especially for the rural areas where there is no access to electricity.

Various studies [7][8][9] show that PCMs have low thermal conductivity that significantly affect the rate of heat transfer in charging/discharging process and the performance of the latent heat storage system. Techniques like using extended surfaces (fins) in the PCM, composites with porous materials, the use of multiple PCMs, micro-encapsulation of PCMs, and a combination of these are used as a solution for the heat transfer enhancement. From these alternatives, fins are easy in manufacturing, usage and maintenance.

Although fins are effective in increasing heat transfer rate, they have also a negative impact on the capacity of thermal energy to be stored. This is due to the reason that when the number of fins embedded in the PCM is increased, the mass of the PCM gets reduced and the amount of thermal energy which is directly proportional to the mass of PCM also reduces. The focus of this study, therefore, is to design, experimental study and getting the optimum fin size for the best heat transfer rate and thermal energy capacity of a solar cooker

1.3   Objectives of the study

1.3.1   Main objective

The main objective of this study is to optimize a design through CFD simulation and experimental validation of a finned phase change material (PCM) thermal energy storage for solar cooking application.

1.3.2   Specific objectives

To meet the main objective the following specific objectives has to be achieved.

- Collecting and assessing solar data of the selected site.
- Specifying and calculating cooking requirements
- Selecting and sizing of appropriate solar collector
- Selecting and sizing of a PCM thermal energy storage.

- Conducting CFD simulation for different fin parameters as input for optimization.
- Parametric optimization for fast heat transfer rate and maximum energy storage capacity.
- Conducting experiment on the thermal energy storage for validation.

1.4 Significance of the research

The importance of this work is to provide a comprehensive information on the utilization of optimized design of a PCM thermal energy storage by integrating with solar cookers. Therefore the outcomes from this study can be important:

- In promoting clean energy utilization by enhancing energy storages.
- For late cooking and water heating.
- To give awareness on phase change material implementation for solar thermal systems.
- In getting continuous energy use and time reduction by using enhanced storages.
- In reducing health hazards of using biomass especially for mothers and child labor.
- As an input/reference for further related studies on the PCM.

1.5 Scope and limitations of the study

The study is limited to the weather condition of the selected area. Sizing and selection were applied for solar collection part and cooking part. The PCM thermal energy storage is designed by applying a mathematical models followed by design optimization of the phase change material using fin parameters. Experiment is used to study the effect of fins in the performance of the storage material. The absence of quality solar reflectors and manufacturing technology has limited the experiment to use artificial heating source.

The CFD simulation and experiment are both parallel studies which makes study more interesting and reliable. The main purpose of the CFD is to investigate the effects of fin and compute the completion time during melting/solidification. While the experiment is to validate the CFD results. In addition to this CFD results are input for the same parameters in the design optimization.

2 Literature Review

2.1 Solar collectors

Solar collectors are the main component of any solar system in which the solar radiation energy is converted to internal energy of the transport medium. It is a section that absorbs the incoming solar radiation, converts it into heat, and transfers the heat to a fluid (usually air, water, or oil) flowing through the collector. Hence it comprises the reflector, absorber and heat transportation medium.

There are two types of solar collectors: non-concentrating and concentrating. A non-concentrating collector has the same area for intercepting and absorbing solar radiation, whereas a concentrating solar collector usually has concave reflecting surfaces to intercept and focus the sun's beam radiation to a smaller receiving area, in this way increasing the radiation flux. Concentrating collectors are suitable for high-temperature applications due to the abundance of the radiation flux at the absorber.

2.1.1 Stationary collectors

Stationary solar collectors are the most commonly used solar collectors in low temperature applications. They are suitable for supplying heat at temperatures up to about 90°C .These collectors are able to collect both direct and diffuse radiation and do not have moving parts as part of the collector [10].

2.1.1.1 Flat plate collectors

Flat plate collector is the simplest and most easily available collector, and is widely used for water heating, space heating and drying applications, which require the temperature of the medium to be less than 100°C. A typical flat plate collector and its components are is shown in figure 5. Any flat plate collector consists of three components: absorber plate, top covers/glazing and heating pipes. Many small-scale flat plate collectors use open/closed loop natural circulation techniques to circulate the heating medium. The absorbers of these collectors are straight copper/aluminum sheets with attached heating pipes [10].
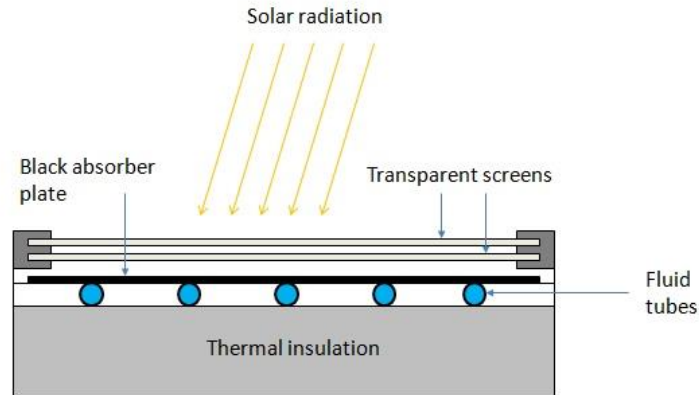
Figure 5. Schematic of a flat plate solar collector with liquid transport medium [11]

2.1.1.2 Evacuated tube collector

Evacuated tube solar collector consists of a heat pipe absorber inside a vacuum-sealed glass tube. The evacuation of air from the glass tube helps to eliminate convection and conduction heat loss but allow the entry of solar radiation to the tube. This type of collector is effective in reheating of water in the recirculation loop of water heaters with very low losses compared to flat plate collectors. This collector produces higher temperature water than flat plate solar collector (>80 °C) [12].

2.1.1.3 Compound parabolic collectors

Compound Parabolic Concentrator (CPC) is a special type of concentrator constructed from the shape of two meeting parabolas. It is a non-imaging concentrator with limited concentrating ratio and it requires only intermittent tracking because of its weak focusing accuracy [10].

2.1.2 Sun-tracking concentrating collectors

In order to increase the temperature of heat transfer fluids from solar collectors it is when heat loss of their receivers has to be reduced and if a large amount of solar radiation can be concentrated on a relatively small receiver area (high concentration ratio). Concentrating collectors have certain advantages over non-concentrating collectors in supplying high temperature, higher thermal efficiency and economic feasibility as a result of small receiver area.

Concentrating collector systems may apply for solar power generation and process heat production because of their capability of higher temperature energy delivery. In spite of the huge potentials for solar thermal concentrators in industrial heat supply, between 50 and 1,500°C, so far they have not been applied for more than 400°C for this purpose. Parabolic trough, parabolic dish and heliostat collectors and offset reflectors (Scheffler type reflector) are the common collectors under this category.

Because of the apparent movement of the sun across the sky, conventional concentrating collectors must follow the sun's daily motion. The sun's motion can be readily tracked by two methods. The first is the altazimuth method, which requires the tracking device to turn in both altitude and azimuth, that is, when performed properly, this method enables the concentrator to follow the sun exactly. Paraboloidal solar collectors generally use this system. The second one is one-axis tracking, in which the collector tracks the sun in only one direction, either from east to west or north to south. Parabolic trough collectors (PTCs) generally use this system. These systems require continuous and accurate adjustment to compensate for the changes in the sun's orientation [13].

2.1.2.1 Parabolic trough collectors

Parabolic trough collector are made by bending a sheet of reflector into a parabolic shape to have a line focus. The line focus commonly uses a black coated pipe receiver that is sometimes covered with a vacuum glass tube to reduce heat losses. This concentrator needs one axis tracking to collect parallel incident rays and reflect them onto the receiver tube. The concentrated reflected radiation reaching the receiver tube converts in to heat and start heating the fluid that circulates through it. Figure 6 shows a schematic of a parabolic collector with vacuum glass covered receiver.
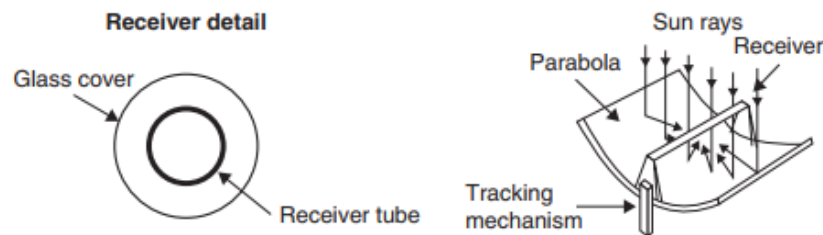
Figure 6. Schematic of a parabolic trough collector and receiver [13]

2.1.2.2 Parabolic dish collector

A parabolic dish reflector is a point-focus collector that tracks the sun in two axes to concentrate solar radiation onto a receiver located at its focal point. The dish fully tracks the sun to collect beam radiation and reflect them onto the receiver. The receiver then absorbs the radiant energy and converts it into thermal energy in a circulating fluid. This thermal energy can be used directly or converted into electricity. This concentrator can achieve temperatures in excess of 1,500°C on its receiver [13]. Figure7 (a) gives the schematic of parabolic dish concentrator.

(a)   (b)
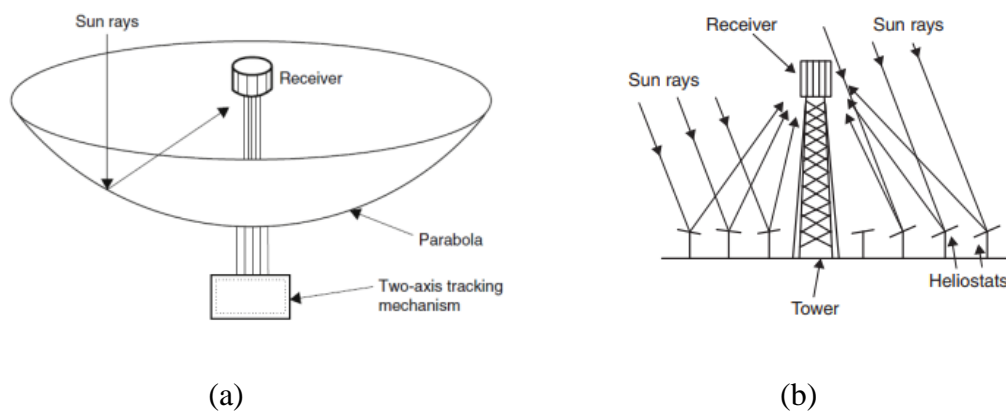
Figure 7. Schematic of parabolic dish collector (a) and central receiver system (b).[13]

Compared to other concentrators parabolic dish concentrators have several advantages as shown below[13].

1. They are the most efficient of all collector systems because of beam radiation collection.
2. Have higher concentration ratios (600–2000) and are efficient thermal energy absorber and convertor.
3. They are modular collectors that can function independently/as part of a larger system of dishes.

2.1.2.3 Heliostat field collector

In heliostat field or central receiver collector, for extremely high inputs of radiant energy, a multiplicity of flat mirrors, or heliostats, using altazimuth mounts can be used to reflect their incident direct solar radiation onto a common target, as shown in Figure 7 (b). By using slightly concave mirror segments on the heliostats, large amounts of thermal energy can be directed into the cavity of a steam generator to produce steam at high temperature and pressure.

In the design for the solar cooking, parabolic trough collector has been selected due to:

- Its low cost.
- Its high temperature range which is suitable for steam generation.
- The advantage of single axis tracking.

In general the solar collectors and their feature are given in table 1.

Table 1. Solar energy collectors [13]

Motion	Collector Type Indicative	Absorber Type	Concentration Ratio	Temperature Range (°C)
Stationary	Flat-plate collector (FPC)	Flat	1	30-80
	Evacuated tube collector (ETC)	Flat	1	50-200
	Compound parabolic collector (CPC)	Tubular	1-5	60-240
Single-axis tracking	Compound parabolic collector (CPC)	Tubular	5-15	60-300
	Linear Fresnel reflector (LFR)	Tubular	10-40	60-250
	Cylindrical trough collector (CTC)	Tubular	15-50	60-300
	Parabolic trough collector (PTC)	Tubular	10-85	60-400
Two-axis tracking	Parabolic dish reflector (PDR)	Point	600-2000	100-1500
	Heliostat field collector (HFC)	Point	300-1500	150-2000

2.2 Phase change materials (PCM)

2.2.1 Desirable characteristics of PCMs

Phase change materials are mostly known by their high heat of fusion for melting in any required temperature range. For this reason, PCMs are available for different temperature range applications. (i.e. Low temperature, medium temperature and high temperature).although it is difficult to get all the desired properties for a single PCM, there has to be certain properties that are suitable for use. The properties can be thermo-physical properties, kinetic and chemical properties, and economic aspects.

The temperature range is one of the main criteria for the suitability of a PCM in any application. There are numerous TES applications that use PCM, which all fit a particular range suitable for their optimum thermal performance.

The main characteristics required for PCMs are summarized shown in table 2.

Table 2. Main desirable characteristics of PCMs

Properties	Desirable characteristics
Thermal properties	Melting temperature in operating range, high heat of fusion, high specific heat, high thermal conductivity of both phases
Physical properties	Small volume change during phase change, high density, small vapor pressure at operating temperatures
Chemical properties	Long term chemical stability with no chemical decomposition, compatible with container material, non-toxic, non-flammable, non-explosive
Kinetic properties	Little or no super cooling during freezing, high nucleation ratio to avoid super-cooling, adequate rate of crystallization
Economics	Abundant, large-scale availabilities, cost effective

A common problem encountered with PCM usage is the lack of a comprehensive database of thermo physical properties, information about long term stability, corrosion, phase segregation, and sub-cooling. However, the most significant shortcoming limiting PCM widespread use in latent heat thermal storage systems is their low thermal conductivity, which typically ranges

from 0.15 - 0.3 W/(m·K) for organic materials, and from 0.4 - 0.7 W/(m·K) for salt hydrates [14].

2.2.2 Phase change materials classification

Latent heat storage materials are broadly classified based on their physical transformation for heat absorbing and desorbing capabilities [15]. A wide range of PCMs has been investigated by several researchers and PCMs are classified as organic, inorganic and eutectics.
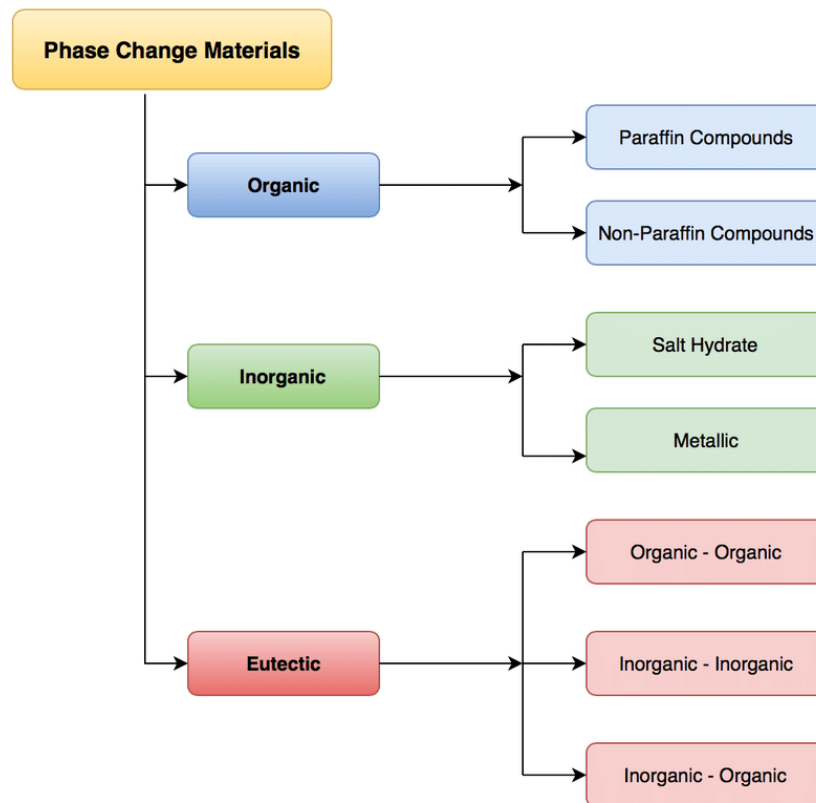
Figure 8. Classification of phase change materials [5]

2.2.2.1 Organic PCMs

These material classes cover the temperature range between 0 ℃ and about 200 ℃. Due to the covalent bonds in organic materials, most of them are not stable to higher temperatures. They are able to melt and freeze repeatedly without phase segregation and consequent degradation of their latent heat of fusion. Moreover, they crystallize with little or no super cooling and they are usually non corrosive. The most important organic PCMs are paraffins, fatty acids and sugar alcohols.

Organic materials can be sub divided into paraffin and non-paraffin.

14

A. Paraffin waxes

Paraffin waxes consist of a mixture of mostly straight chain n-alkenes CH3—(CH2)—CH3. The crystallization of the (CH3)— chain releases a large amount of latent heat. Both the melting point and latent heat of fusion increase with chain length. Owing to cost consideration, however, only technical grade paraffins could be used as PCMs in LHS systems. Paraffin is safe, reliable, predictable, less expensive, noncorrosive, and available in a large temperature range (5°C-80°C) [5].

B. Non‑paraffin organic PCMs:

These organic categories are the most numerous of the PCMs with highly varied properties. A number of esters, fatty acids, alcohols, and glycols suitable for energy storage have been identified. Some of the main features of these organic materials include high heat of fusion, inflammability, low thermal conductivity, low flash points, and instability at high temperatures.

Fatty acids have a high heat of fusion compared with paraffins, and they have reproducible melting and freezing behaviors with little or no super-cooling. However, fatty acids are more expensive than technical grade paraffins, and they are mildly corrosive and possess an unpleasant odor [15][5].

Table 3. Thermo-physical properties of selected organic compounds [15].

Compound	Melting Point, °C	Melting Enthalpy, kJ/kg	Specific Heat, kJ/(kg·K)		Thermal Conductivity, W/(m ·K)		Density, kg/m^3
			Solid	Liquid	Solid	Liquid	
Formic acid	8	277	1.00	1.17	0.30	0.27	1227
Acetic acid	17	192	1.33	2.04	0.26	0.19	1214
Lauric acid	44	212	2.02	2.15	0.22	0.15	1007
Stearic acid	54	157	1.76	2.27	0.29	0.17	940
Palmitic acid	61	222	1.69	2.20	0.21	0.17	989
Parrafin wax	0-90	150-250	3.00	2.00	0.20	–	880-950
Acetamide	82	260	2.00	3.00	0.40	0.25	1160
Erythritol	117	340	2.25	2.61	0.73	0.33	1450
HDPE	130	255	2.60	2.15	0.48	0.44	952
Urea	134	250	1.80	2.11	0.80	0.60	1320
Maleic acid	141	385	1.17	2.08	–	–	1590
d-Mannitol	165	300	1.31	2.36	0.19	0.11	1490
Hydroquinone	172	258	1.59	1.64	–	–	1300

2.2.2.2 Inorganic PCMs

Inorganic PCMs are used in high-temperature solar applications and one of their most reported challenges is maintenance. At low temperatures, they freeze, and at high temperatures, they are difficult to handle. These PCMs do not super-cool appreciably, and their melting enthalpies do not degrade with cycling. The two main types are as follows [15].

A. Salt hydrates

Salt hydrates with the general formula AB·nH2O are alloys of inorganic salts (AB) containing *n*kmol of water of crystallisation. During phase transformation, dehydration of the salt occurs, forming either a salt hydrate that contains fewer water molecules:

$$AB.nH_2O \rightarrow AB.mH_2O + (n-m)H_2O \qquad (4)$$
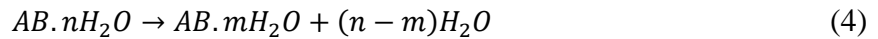
or to its anhydrous form:

$$AB.nH_2O \rightarrow AB + nH_2O \qquad (5)$$

At the melting point the hydrate crystals breakup into anhydrous salt and water, or into a lower hydrate and water. One problem with most salt hydrates is that of incongruent melting caused by the fact that the released water of crystallization is not sufficient to dissolve all the solid phase present. Due to density difference, the lower hydrate (or anhydrous salt) settles down at the bottom of the container.

Table 4. Thermo-physical properties of selected salt hydrates [15]

Compound	Melting Point, °C	Melting Enthalpy, kJ/kg	Specific Heat, kJ/(kg·K)		Thermal Conductivity, W/(m ·K)		Density, kg/m³
			Solid	Liquid	Solid	Liquid	
Water	0	333	3.30	4.18	1.60	0.61	920
Calcium chloride hexahydrate	30	125	1.42	2.20	1.09	0.53	1710
Sodium sulphate decahydrate	32	180	1.93	2.80	0.56	0.45	1485
Sodium thiosulfate pentahydrate	46	210	1.46	2.39	0.76	0.38	1666
Sodium acetate trihydrate	58	265	1.68	2.37	0.43	0.34	1450
Barium hydroxide octahydrate	78	280	1.34	2.44	1.26	0.66	2180
Magnesium nitrate hexahydrate	89	140	2.50	3.10	0.65	0.50	1640
Oxalic acid dihydrate	105	264	2.11	2.89	0.90	0.70	1653
Magnesium chloride hexahydrate	117	150	2.00	2.40	0.70	0.58	1570

Salt hydrates are the most important group of PCMs, which have been extensively studied for their use in latent heat thermal energy storage systems. The most attractive properties of salt hydrates are the high latent heat of fusion per unit volume, relatively high thermal conductivity (almost double of the paraffin's), and small volume changes on melting. They are not very corrosive, compatible with plastics and only slightly toxic. Many salt hydrates are sufficiently inexpensive for the use in storage [16].

B. Metallics

This category includes the low melting metals and metal eutectics. These metallics have not yet been seriously considered for PCM technology because of weight penalties. However, when volume is a consideration, they are likely candidates because of the high heat of fusion per unit volume. They have high thermal conductivities, so fillers with added weight penalties are not required. The use of metallics poses a number of unusual engineering problems. A major difference between the metallics and other PCMs is their high thermal conductivity [5].

Some of the features of these materials are: low heat of fusion per unit weight, high heat of fusion per unit volume, high thermal conductivity, low specific heat and relatively low vapor pressure.

2.2.2.3 Eutectics

Eutectic materials are combinations of two or more low melting point materials with similar (congruent) melting and freezing points; eutectics nearly always melt and freeze without segregation and have high thermal conductivities and densities. The weight percentage of each material can be varied to obtain different melting points of the resulting eutectic mixture. For this reason, they are a promising type of PCM for the future, even if they are actually less diffused than the other groups. The problem with eutectics is they have low latent heat and specific heat capacities.

Table 5. Thermo-physical properties of selected eutectic compounds [15]

| Compound	Mass Ratio	Melting Point, °C	Melting Enthalpy, kJ/kg	Specific Heat, kJ/(kg·K)		Thermal Conductivity, W/(m·K)		Density, kg/m³
				Solid	Liquid	Solid	Liquid	
$CaCl_2 \cdot (H_2O)_6 MgCl_2 \cdot (H_2O)_6$	67-33	25	127	1620	2270	0.930	0.550	1661
Urea $CH_3COONa \cdot (H_2O)_3$	60-40	30	200	1750	2210	0.630	0.480	1370
$Mg(NO_3)_2 \cdot (H_2O)_6 NH_4NO_3$	61-39	52	125	2130	2670	0.590	0.500	1672
Urea-acetamide	38-62	53	224	1920	2660	0.510	0.340	1216
$Mg(NO_3)_2 \cdot (H_2O)_6 - MgCl_2 \cdot (H_2O)_6$	59-41	59	132	2290	2810	0.670	0.530	1610
Stearic acid - acetamide	83-17	65	213	1800	2400	0.300	0.180	972
$LiNO_3 MgNO_3 \cdot (H_2O)_6$	14-86	72	180	2380	2900	0.700	0.510	1713
Urea-$LiNO_3$	82-18	76	218	1770	2020	0.850	0.600	1438
Urea-$NaNO_3$	71-29	83	187	1600	2030	0.750	0.590	1502
Urea-NH_4Cl	85-15	102	214	1770	2090	0.760	0.580	1348
Urea-K_2CO_3	15-85	102	206	1660	2020	0.780	0.580	1415
Urea-KNO_3	77-23	109	195	1600	1910	0.810	0.580	1416
Urea-NaCl	90-10	112	230	1720	2020	0.820	0.600	1372
Urea-KCl	89-11	115	227	1690	1960	0.830	0.660	1370
KNO_3-$NaNO_2$	56-44	141	97	1180	1740	0.730	0.570	1994
KNO_3-$NaNO_3$-$NaNO_2$	53-6-41	142	110	1170	1730	0.720	0.570	2006
KNO_2-$NaNO_3$	48-52	149	124	1050	1630	0.580	0.520	2080
$LiNO_3$-$NaNO_2$	62-38	156	233	1570	1910	1.120	0.660	2296
$LiNO_3$-KCl	58-42	160	272	1260	1350	1.310	0.590	2196
$LiNO_3$-$NaNO_3$-KCl	45-50-5	160	266	1320	1690	0.880	0.590	2297
LiOH-$LiNO_3$	19-81	183	352	1600	2000	1.330	0.690	2124
$LiNO_3$-$NaNO_3$	49-51	194	262	1350	1720	0.870	0.590	2317
$LiNO_3$-NaCl	87-13	208	369	1540	1560	1.350	0.630	2350
KNO_3-KOH	80-20	214	83	1030	1350	0.880	0.540	1905
KNO_3-$NaNO_3$	55-45	222	110	1010	1490	0.730	0.510	2028
LiBr-$LiNO_3$	27-73	228	279	1340	1380	1.140	0.570	2603
LiOH-$NaNO_3$-NaOH	6-67-27	230	184	1300	2000	0.780	0.670	2154
$NaNO_2$-$NaNO_3$	55-45	233	163	1310	2130	0.590	0.640	2210
$CaCl_2$-$LiNO_3$	13-87	238	317	1500	1530	1.370	0.690	2362
LiCl-$LiNO_3$	9-91	244	342	1580	1610	1.370	0.640	2351
$NaNO_3$-NaOH	86-14	250	160	1190	1860	0.660	0.600	2241

2.2.3   Hitec salt Properties

2.2.3.1   Physical properties

The heat transfer salt (HTS), Hitec, marketed by Coastal Chemical Co. (a DuPoint subsidiary), contains 40% $NaNO_2$, 7% $NaNO_3$, and 53% KNO_3 by weight. This mixture melts at 142°C, but appreciable changes in composition do not affect the freezing point markedly. HTS has essentially zero vapor pressure in the 142 to 450°C range, and its specific heat is appreciably lower than that of water (approximately, 1/3). However, its thermal conductivity is approximately the same and its density is approximately twice as large. The viscosity of HTS in its useful temperature range is greater than that of water and the liquid metals by an order of magnitude, but it compares favorably with other heat transfer fluids on the basis of heat-transport capacity (the heat transferred per unit time, over a given range of temperature, for varying mass velocity) [17].

HTS possesses most of the desirable attributes required for a heat transfer medium. HTS has a low melting point, although impurities formed by thermal decomposition (largely from $NaNO_2$) gradually elevate the melting point. The salt mixture is stable in air and in the presence of moisture. It is relatively nontoxic and is nonflammable; however, the molten salt must be kept out of contact with easily oxidized organic materials. Hitec does not explode spontaneously. However, the molten salt must be prevented from coming into contact with hot carbon since the mixture explodes.

2.2.3.2   Chemical properties

The chemistry of the thermal stability of HTS is complex but that the decomposition of HTS proceeds through several significant reactions involving sodium nitrite (the least stable component of the three compounds that form heat transfer salt). However, the generally accepted Overall reaction for its decomposition is:

$$5NaNO_2 \rightarrow 3NaNO_3 + Na_2O + N_2 \tag{6}$$
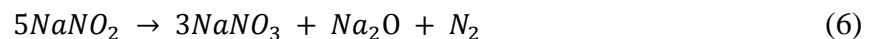
Nitrogen evolution measurements and the above stoichiometry have been employed to estimate the decomposition of Hitec heat transfer salt with time and as a function of temperature. Although these data indicate that a Hitec heat transfer salt system operating between 260 and 520°C might require replacement of about half the nitrite in the mixture annually, industrial experience has been much more favorable. One circulating Hitec heat transfer salt system has been operated under a nitrogen purge at temperatures up to

~500°C for about five years with "minimal" incident and "minor" salt replacement. Another installation believes 10 years of operation at approximately 480 to 510°C under such conditions is achievable. It has been reported that the decomposition of alkali nitrate-nitrite mixtures is catalyzed by iron above 520°C but not by stainless steel. Because the only long-term (18 to 30 months) quantitative data presented were obtained in carbon steel circulation loops, the long-term stability of Hitec heat transfer salt (of varying purity) should be investigated at elevated temperatures (450 to 550°C) in low-alloy steel and stainless steel systems [17].

2.3 Heat transfer enhancement techniques of PCMs

Except the metallic type PCMs, all classes of pure PCMs have a low thermal conductivity which makes them poor in the performance of latent thermal energy systems, although inorganic PCMs have comparatively higher thermal conductivities than organic ones. This low thermal conductivity property of the material leads to reduced heat exchange between the PCM and the HTF.

This is a big challenge in the thermal energy storage systems. In order to overcome this challenge, numerous techniques has been developed. The most common enhancement methods are:

- ➢ Extended surfaces (fins)
- ➢ Composite PCMs (thermal conductivity enhancement)
- ➢ Multiple PCMs
- ➢ PCM Encapsulation

2.3.1 Extended surfaces

Fins or extended surfaces provide additional heat transfer surface area which consequently enhances the heat transfer rate in thermal systems. Various shapes and configurations of fins to be employed in LHTES systems has been reported by researchers.

The common configurations of LHTES investigated so far are of two kinds:

i.   System that involves heat storage and retrieval through hot/cold HTF, such as the one used in solar air or water heaters. and

ii.   System that serves as a heat sink reservoir through hot/cold boundary wall, for example, the ones used in electronic cooling.

In heat sink based-LHTES systems, which do not involve HTF, the fins are located within the PCM. However, the fins location in LHTES with HTF is generally on the side with lower relative thermal conductivity, which in most cases is the PCM [7].

2.3.2 Composite PCMs

In this technique, thermal conductivity of PCMs is improved by impregnation of porous materials of high thermal conductivity, dispersion of high conductivity materials or nanoparticles and dispersion of low-density materials into the base PCM. This enhances the overall thermal performance of LHTES systems [7]. Graphite is known for its high thermal conductivity, high electrical conductivity and high absorbability and as result various types of graphite are used in latent heat storage materials like natural graphite flakes, expanded natural graphite and ground expanded natural graphite[18].

2.3.3 Multiple PCMs

The other technique for performance enhancement is the use of cascaded or multiple types of PCMs in LHTES systems. The purpose of multiple PCMs is to maintain a nearly constant temperature difference between the HTF and the PCMs during charging and discharging cycles, thereby increasing the thermal performance of the system.

A shell and tube device employing both cascaded salts with internal fins as shown figure 9 containing 5 PCMs, gave better melting process in comparison with the use of single PCM by [19]. In addition to that, using the finned structure on the basis of cascaded salts arrangement gave a significant performance enhancement, and almost uniform HTF outlet temperature.
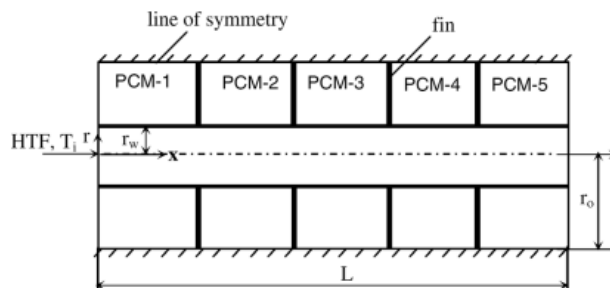

Figure 9. Multiple PCMs in shell-and-tube LHTES unit.

2.3.4   Microencapsulation of PCM

In this method micro and Nano size PCM particles are enclosed in a sphere or cylinder. PCM inside the capsule is known as core and capsule in solid structure as shell. The shell can be made of wide range of materials including natural and synthetic polymers. Microencapsulation of PCMs can be made by two methods namely chemical and mechanical or physical methods.

Due to large heat transfer area per unit volume of the container, microencapsulated PCMs can be expected to present higher transfer rate than that of pure PCMs [8].

2.4   Design Optimization

2.4.1   Introduction

In the field of engineering, there is continuous need to improved products, processes and designs. This requires a wise decision making for considerations like competitive product in the market and performance aspects. Therefore optimization is the process of determining the best design.

Genetic Algorithm or Evolutionary Algorithms have proven to have a global perspective of the design space in finding optimal solutions and have been used for optimization of engineering problems for several years. Evolutionary or Genetic Algorithms mimic evolutionary principles observed in nature such as natural selection, reproduction, crossover and mutation. The idea behind this method is that, an initial population of designs are generated within the design space by principles of crossover and mutation. These designs are then evaluated, and their output responses are used as performance metrics of each design. If the goal is to minimize an output response, the design with the least value of output will be ranked highest (strongest) in the population. Correspondingly, the design with the most value of the output will be ranked the lowest (weakest).

A selection procedure is used to eliminate weaker designs and reproduction will ensure parameters from the stronger designs are passed onto the next generation. This procedure of crossover, mutation, selection and reproduction is carried out over generations of populations till either the solution doesn't change anymore, or maximum number of generations have been evaluated. According to evolution theory, with every passing generation, a species becomes better at adapting to the surroundings. The reasoning is that, weaker entities within a generation are eliminated and

traits from the stronger entities are passed onto the next generation which help the successive generations to become better at survival.

2.4.2   Response surface methodology

Response surface methodology (RSM) is a collection of mathematical and statistical techniques useful for the modelling and analysis of problems in which a response of interest is influenced by several variables and the objective is to optimize this response [20]

In most RSM problems, the form of the relationship between the response and the independent variables is unknown. Thus, the first step in RSM is to find a suitable approximation for the true functional relationship between the response and set of independent variables. If the response is well modelled by a linear function of the independent variables, then the approximating function is the first order model.

$$y = \beta_0 + \beta_1 x_1 + \beta_2 x_2 + \cdots \beta_k x_k + \epsilon \tag{7}$$

If there is a curvature in the system, then a polynomial of higher degree must be used, such as the second order model,

$$y = \beta_0 + \sum_{i=1}^{k} \beta_1 x_1 + \sum_{i=1}^{k} \beta_{ii}\, x_i{}^2 + \sum_{i<j}\sum \beta_{ii}\, x_i\, x_j + \epsilon \tag{8}$$

The response surface analysis is then performed using the fitted surface and this fitted response surface is then used for optimizing the input variables versus output responses. If the fitted response surface is an adequate approximation of the response function, then analysis of the fitted surface will be approximately equivalent to the analysis of the actual system. A response surface is approximated for each output response.

Coefficient of determination (R^2) is used to analyze the goodness of fit for each response surface. Coefficient of determination is the percent of the variation of the output parameter that can be explained by the response surface model.

The model coefficients (weights) from the first or second order models can be estimated most effectively if proper experimental/simulation designs are used to collect data. Designs for fitting response surface are called response surface designs.

2.4.3   Multi-objective optimization

Designing a latent heat energy storage system will require the design to be maximized energy storage capacity and fast responsive. Thus, the objective of this optimization study was to minimize the CFD melt time of the PCM and, to maximize the energy storage capacity of the PCM. Based on a general understanding of the system, these two objectives are contradictory. Thus, it is not possible obtain a single optimum solution. Instead there will be a population of optimal solutions defined as the pareto optimal solutions. This is called Multi-objective Optimization.

Unlike single objective optimization, in multi-objective optimization, designs that improve one objective worsen another objective. Consider, a PCM and dispersed fins filled in a cylinder. If the length and thickness of the fins inside the PCM are increased, then the time for melting as well as solidification will be shorter. But this reduces the amount of the PCM, consequently the heat capacity (energy storage) will be reduced. Thus, increasing fin dimensions results in decreasing the melt time and vice-versa. Therefore, in case of multi objective optimization, there is no clear optimum solution. But there will be these many optimal solutions that form a pareto front and the purpose of a multi-objective optimization is to improve this pareto front.

2.5   Related Works

Buddhi and Sahoo [21] designed and tested a box type-solar cooker integrated with latent heat storage for late evening cooking. In their design, Commercial grade stearic acid (melting point 55 °C, latent heat of fusion 161 kJ/kg) as PCM was filled below the absorbing plate. The PCM was selected due to its low cost and availability. It was found that the rate of heat transfer from the PCM to the cooking pot during the discharging/solidification mode of the PCM is slow and more time is required for cooking in the evening. In addition, they recommended the increasing size of insulation can reduce the size of the storage. In their work, there was no attempt of heat transfer enhancement like incorporating fins in the storage that could have been better design.

Sharma et al. [22] developed a solar cooker which is evacuated tube solar collector (ETSC) type integrated with PCM storage as shown in Figure 10. It consists of an ETSC, a PCM storage unit, cooking unit, a closed loop pumping line with water as heat transfer fluid (HTF), pump, relief valve, flow meter and a stainless steel tubular heat exchanger. The PCM storage unit consists of two hollow concentric aluminum cylinders in which the space between the cylinders is filled with

45 kg erythritol (melting point 118 °C, latent heat of fusion 339.8 kJ/kg) as the PCM and the inner cylinder space is for cooking pot. A pump is used for circulating the heated water as HTF from the ETSC through the insulated pipes to the PCM storage unit by using stainless steel tubular heat exchanger that wraps around the cooking unit by closed loop.

 In the course of sunshine hours, the hot water transfers its heat to the PCM and stored in the form of latent heat, using the stainless steel tube as heat exchanger. The stored heat is utilized for cooking food in the evening or when sun intensity is not sufficient for cooking. In their conclusion, two times cooking (noon and evening) is possible in a day. Noon cooking did not affect the cooking in the evening and evening cooking using PCM storage was found faster than noon cooking. Although, the experiment and analysis of the prototype solar cooker gave satisfactory performance, the heat transfer was low. This work lacks heat transfer enhancement.
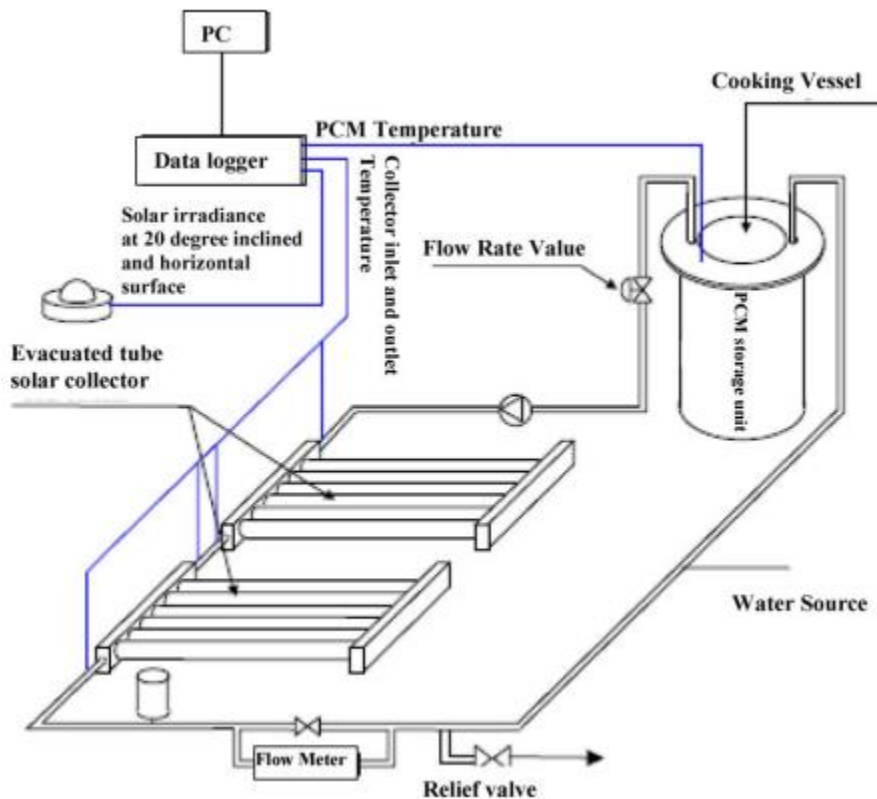

Figure 10. Latent heat storage type evacuated tube solar cooker using erythritol as PCM [22].

Hussein et al. [23] developed a novel indirect solar cooker with outdoor elliptical cross-section wickless heat pipes, flat-plate solar collector with an integrated indoor PCM thermal storage and cooking unit as shown in Figure 11. Two plane reflectors are used to enhance the insolation falling

on the collector, whereas magnesium nitrate hexahydrate (melting temperature 89 °C, latent heat of fusion 134 kJ/kg) is used as the PCM inside the indoor cooking unit of the cooker. They studied the performance enhancement of the cooker as the result of the adding plane reflectors to the flat plate solar collector and they found that the average daily enhancement in the solar radiation incident on the collector surface by the south and north facing reflectors is about 24%. It was also found that the use of elliptical cross-section wickless heat pipes and PCMs in indirect solar cookers to cook food at noon and evening and to keep food warm at night and in early morning was successful. The study has not explanations on the special treatment of the PCM material and its heat transfer enhancement.
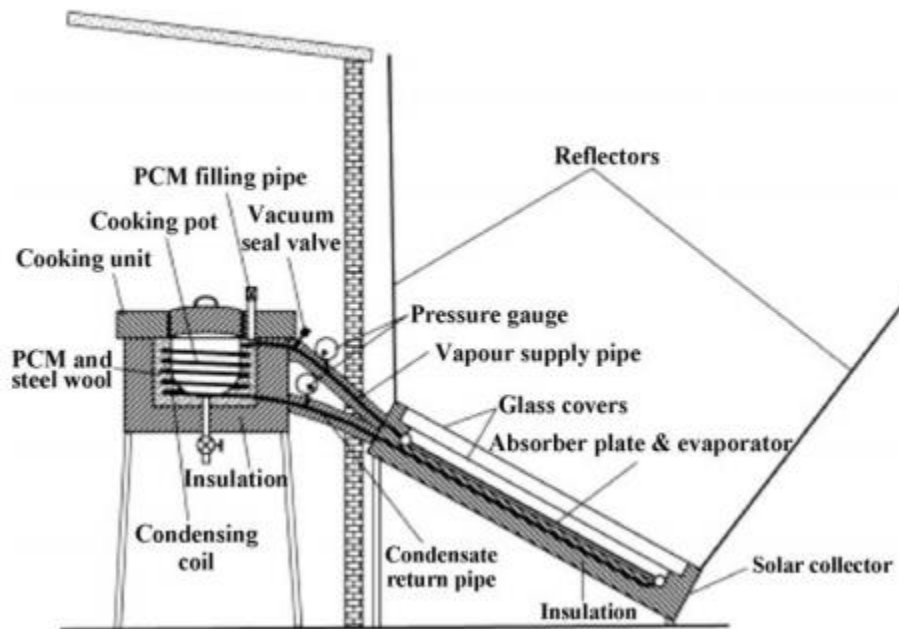
Figure 11. Cross sectional side view of flat plate solar cooker and its components [23].

R.M. Muthusivagami et al. [24] in their study for higher temperature cooking developed a solar cooker with PCM A-164 as energy storage and indoor cooking unit as shown in figure 12. A parabolic trough is used for concentrating solar energy. Thermic fluid was used as heat transfer fluid to exchange the heat between the collector and the cooking unit. PCM A-164 filled in 1 m long, 22 mm diameter tubes will be made as a heat exchanger to store the energy during sunshine hours and to retrieve the energy during off-sunshine hours. The cooking unit is the flat surface hot plate, which is similar to the hot plate employed in the electric cooking. Oil will be circulated below the finned hot plate to keep the surface temperature around 140–150 °C.

It was suggested that, even though the initial investment needed for the system is high due to PCM cost, in the long run it becomes cost effective if the PCM at this temperature range is made available at a lower price. The study has not provided the heat transfer enhancement techniques in the PCM. The complexity of the system as a result of both cooking unit and storage unit are located far apart, there will heat loss.
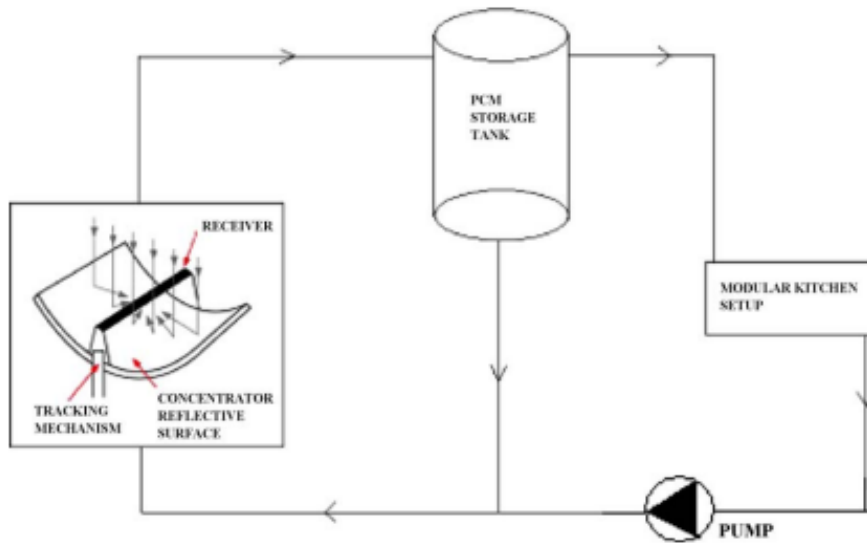
Figure 12. Latent heat storage type concentrating solar cooker using PCM A-164 [24].

Stritih [25] compared the heat transfer characteristics of a rectangular latent heat storage system with and without fins experimentally for solidification and melting processes using paraffin (melting point of 30 °C) was as a PCM. Paraffin is selected because it is appropriate for thermal storage applications in buildings. In conclusion it was found that natural convection was the dominant heat transfer mode during melting and the presence of fins showed insignificant effect on the melting rate, while conduction was the dominant mode of heat transfer during the solidification process. Despite the parametric investigations of fins which affects the heat storage capacity, it has shown about 40% reduction in solidification time due to the presence of fins.

Yang et al. [25] conducted a numerical analysis on performance of naphthalene phase change thermal storage system in aluminum plate-fin unit and found that thermal storage with internal fins gives better thermal performance compared to one without internal fins. Fins in the aluminum plate-fin thermal storage have been accelerated the heat transfer rate. They have concluded Fins improve the energy storage and release performance and smaller fin pitches lead to a shorter

melting/solidification period mainly due to the smaller PCM volume and larger heat transfer surface. The effect of PCM mass reduction as the replacement of fins and optimization has not been investigated which contributes significant effect in the latent energy storage.

S. Mat et al. [26] studied the melting process of a phase change material RT82 in a triplex-tube heat exchanger (TTHX) system which consists three concentric cylinders. Enhancement techniques were compared with the inside tube heating, outside tube heating, both tube heating for melting/charging. The configurations are shown in figure 13, which considers the fin to be on the internal, external or both tubes. The effects of fin length on the enhancement techniques were investigated. Comparative analysis showed that there was no significant difference among the three configurations in terms of PCM melting rate. The use of internal– external fin reduced the time for complete melting of the PCM by 43.3% as compared with that of TTHX without fins. The variation of fin size has not been explained in their work.
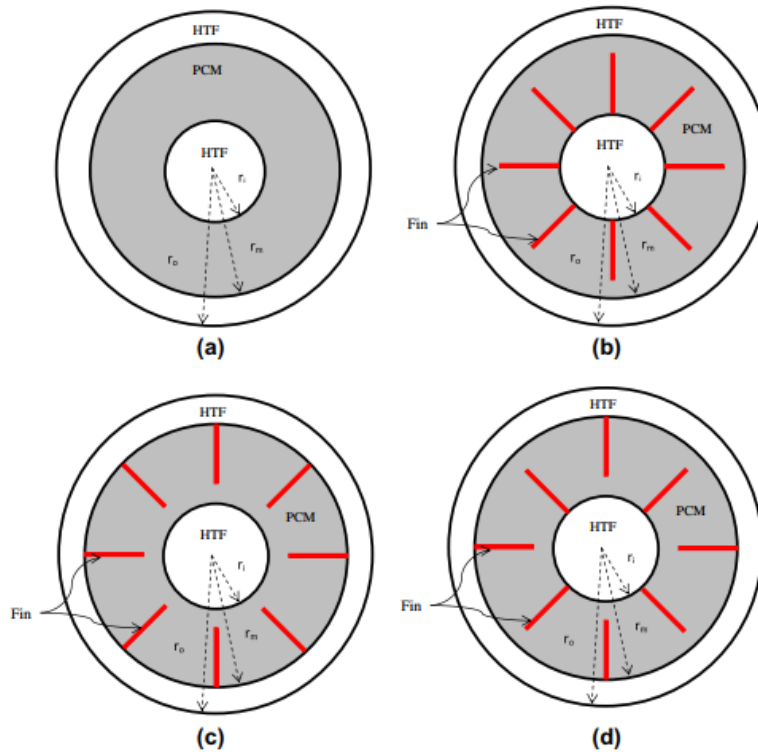
(a) TTHX without fin, (b) TTHX with internal fins, (c) TTHX with external fin, (d) TTHX with internal–external fins.

Figure 13. Model physical configuration [26].

J.M. Mahdi, E.C. Nsofor [27] has studied numerically a triplex-tube configuration with internal-external fins with nanoparticles. The configuration was selected due to the both-sides heating approach that is applied on the annulus housing of the PCM, allows the PCM to have a larger heat-exchange area in comparison to the common double-pipe heat exchanger. They reported that the use of fin-nanoparticle combinations showed better solidification effect than using nanoparticles alone and recommends to increase the fin length and decrease the fin thickness to improve the PCM thermal response for solidification in longitudinally-finned latent heat storage systems.

Lohrasbi et al. [28] conducted numerical investigation on discharging process of PCM in cylindrical reservoir containing PCM.it was reported that employing fin in PCM storage system is a significantly efficient enhancement technique for discharging rate. Fin geometry parameters has also shown a significant effect on energy storage performance, but they didn't carry out optimization to give the best fin structure.

In general, most of the literatures has focused on the heat transfer enhancement of thermal energy storages. The most important method for the enhancement is by using fins since it is easy in manufacturing, cost and maintenance. Besides different Phase change materials has been used by matching with the type of solar collector used. The research gap here is that the use of fins in PCMs for heat transfer enhancements are affecting the amount of energy storage which needs a significant treatment in designing thermal energy storages. In addition to this, the application area of the phase change materials is large and there is continuous effort to test in different application areas which this study implements a PCM which hasn't been used for cooking.

3 Materials and Methods

3.1 Study area description

The study area-Jimma zone is located in the Oromia National Regional State, Southwest Ethiopia (Figure 14). Jimma town is the capital and administrative center of the Zone and is located at a distance of 350 km away from the capital of Ethiopia- Addis Ababa [29]. It is located at geographical coordinates of 7.6739° N-latitude, 36.8358° E-longitude and at an altitude of 1780 m above mean sea level.
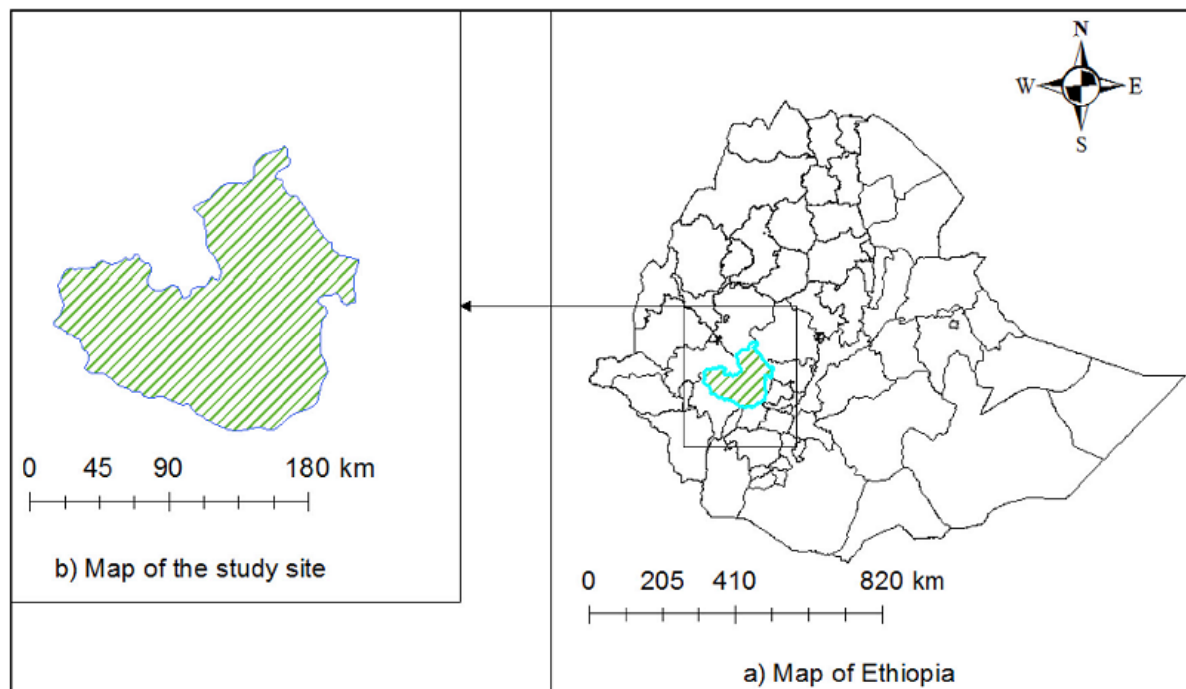
Figure 14. Geographical location of the study area-Jimma Zone in Ethiopia. [30].

It has been important to have some background information on cooking and energy demand of the study area. For this reason questionnaires has been prepared to estimate the average population living per household, the cooking demand, the costs spent for energy supply of the cooking and the background knowledge on existence of solar cooking.

There are 32,191 number of households in Jimma zone [29]. For the present study, a sample of 195 households has been selected according to the sample size calculation [31], considering 95% confidence level and confidence interval of 7.

3.2 Working Principle of the System

The system consists of a parabolic trough solar collector (PTSC), cooking unit which is integrated with the thermal storage and fluid transport pipes. In addition to these major components, insulations, flow control systems and measurement devices take part in the system construction.

The system operates with a closed loop thermosyphon principle of fluid flow. The first step in the system operation is collecting the required amount of heat from the parabolic trough solar collector in the form of steam. The steam then goes to the cooking unit through inlet pipe and once it reaches the copper coil it will be used for cooking and charging the thermal storage. If the user cooks during sunshine period, both cooking and energy storing will be simultaneous. Otherwise the storage system keeps charging during off duty condition. After cooking and charging, the steam will lose its temperature and starts to condensate. This makes the fluid denser and it comes back to the PTSC by the return pipes. This completes the system cycle. Flow regulating valve is also used at the outlet of the solar collector.
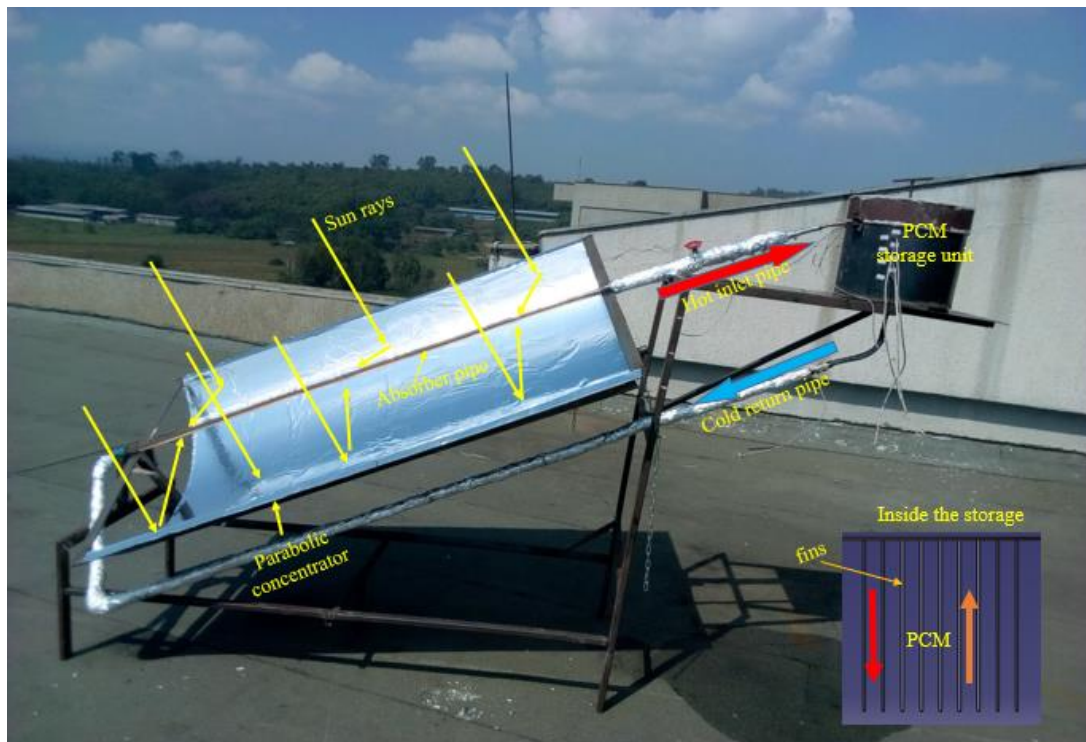
Figure 15. The parabolic trough solar collector integrated with storage unit.

3.3 Experimental set up and materials

3.3.1 PCM preparation

The PCM material was prepared by combining and well mixing of 53% KNO_3, 6% $NaNO_3$ and 41% $NaNO_2$ in Composition.

(a) chemicals   (b) mixing process
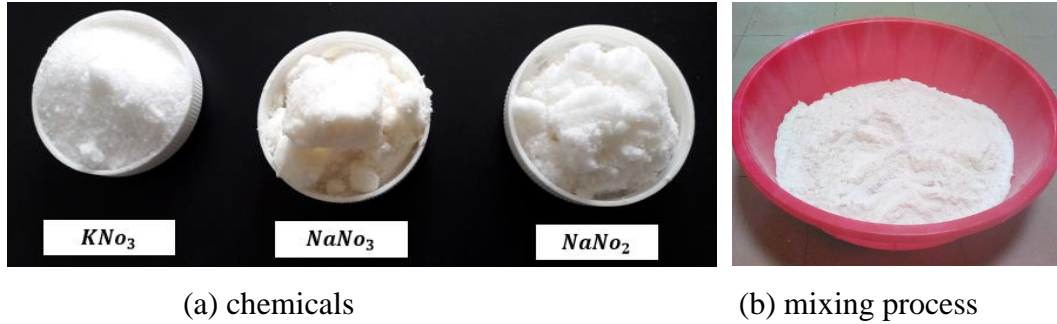
Figure 16. The PCM preparation process

The PCM is then heated up in electric stove until it completely melts. The temperature during the melting process were reached around 540 K well above the melting temperature of the PCM. This makes the PCM in the sensible region and after pouring into the storage cylinder there will be some temperature drop which is expected. Then the time to record temperature measurements was when it reaches 500K which makes the experiment controlled. The storage cylinder is made from two concentric mild steel sheet metal in which the space between the cylinders is filled with ash for insulation. The bottom part is also insulated with ash by extending the length of the outer cylinder. The fins are attached on the pan.
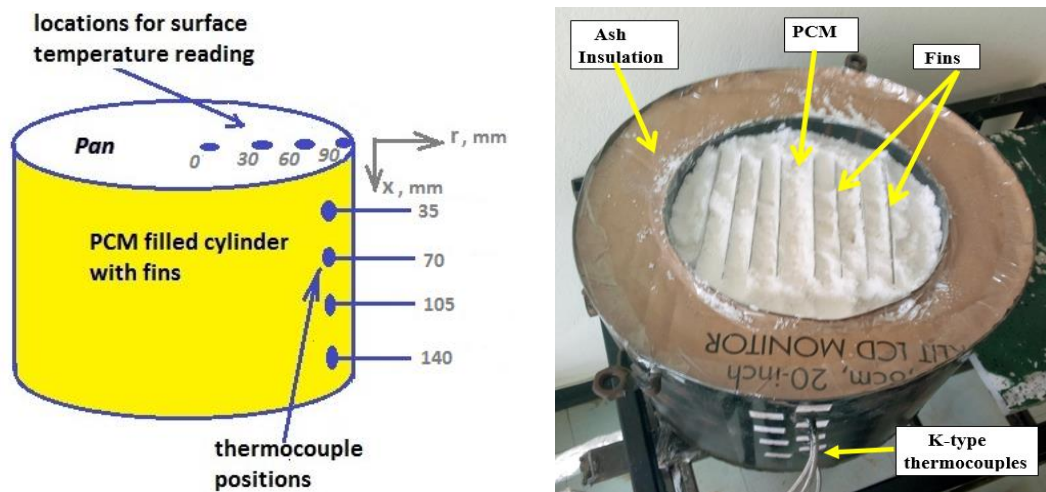
Figure 17. Schematic and physical description of storage system and thermocouple locations.

Temperature measurements were taken using K-type thermocouple sensors from eight (8) locations. Four points are selected radially in the cooking plate and four are positioned along the PCM storage (vertically) unit.

Different thermometers were used in recording data. Mercury thermometers were used for room temperature measurement, Infrared (non-contact type) thermometer for the pan and thermocouples read by multi meters in the PCM storage. Standard watch was used for time measurement.

Figure 18. Devices in temperature measurements

3.4   Fin Design Points

In the design process for the fin parameters, fins thickness and length are taken based on the most common available aluminum sheet metals for the ease of usage. The design points are shown in table 6.

Table 6. Design points

Case	Length (L) in mm	Thickness (t) in mm	Width (w) in mm
1	70	0.8	130
2	70	1	130
3	70	1.5	130
4	105	0.8	130
5	105	1	130
6	105	1.5	130
7	140	0.8	130
8	140	1	130
9	140	1.5	130

Figure 19. Fins thickness used in experiment

3.5 Methods in CFD analysis

The melting and solidification processes were numerically modelled using commercial CFD software ANSYS Fluent 16.0. An enthalpy-porosity technique[32][33]. Is used in FLUENT for modeling the solidification/melting process. In this technique, the melt interface is not tracked explicitly. Instead, a quantity called the liquid fraction, which indicates the fraction of the cell volume that is in liquid form, is associated with each cell in the domain. The liquid fraction is computed at each iteration, based on an enthalpy balance. The mushy zone is a region in which the liquid fraction lies between 0 and 1. The mushy zone is modeled as a \pseudo" porous medium in which the porosity decreases from 1 to 0 as the material solidifies. When the material has fully solidified in a cell, the porosity becomes zero and hence the velocities also drop to zero [34].

3.5.1 Geometry for modelling

The geometry of the fined PCM inside the cylindrical container for numerical simulations is created using ANSYS Design Modeler as shown in Figure 20. The Geometry represents half of the 2D model. The system is modeled as 2D, since the main heat flow is in the longitudinal direction and the variation of fin dimensions is the length and thickness which considers constant fin depth. Being 2D reduces the computing time and power as well as the space of computing machine over 3D. The thickness of the aluminum fins are 0.8, 1 and 1.5 mm with a varying length of 70, 105 and 140 mm.
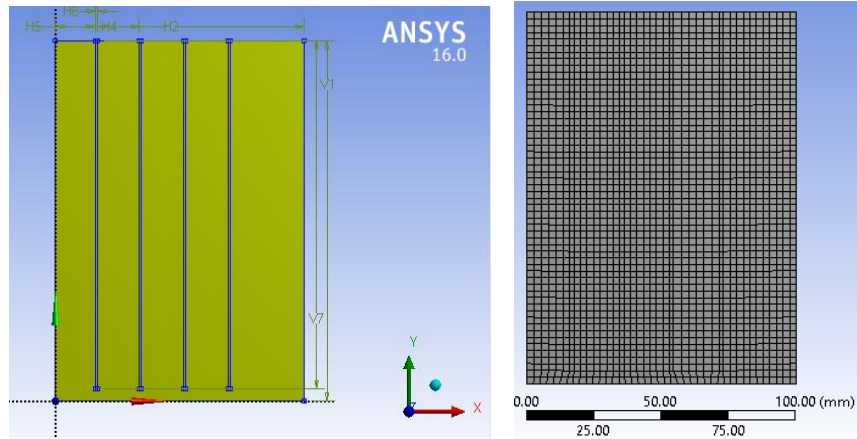
Figure 20. ANSYS 2D-model and meshing.

3.5.2 Meshing

The geometry created in Design Modeler was discretized using ANSYS Mesher. The PCM is considered as fluid domain and the fin is solid domain. For better accuracy the grid size is set to fine. The number of nodes and elements are 2394 and 2296 respectively.

3.5.3 CFD setup and solution

The Boundary and Initial conditions assumptions are as follows.

- The natural convection effects are modeled by the Boussinesq approximation.

- The gravitation forces are considered in the model.

- During modelling the melting process, the initial temperature is set as a constant and uniform at 300 K and for modelling the solidification, the initial temperature is set as constant and uniform at 500 K.

- For melting the boundary conditions given are constant temperature at the pan or top of the PCM and insulated wall, while the symmetry line is kept symmetry.

- For solidification, the upper surface of the PCM is exposed to mixed convection and radiation with convective heat transfer coefficient of $25W/m^2.K$ at ambient temperature of 300 K. the rest are default setting for radiation with 0.002m aluminum pan thickness.

ANSYS FLUENT solves the energy and momentum using the following governing equations.

35

Energy Equation: The enthalpy of the material is computed as the sum of the sensible enthalpy, h, and the latent heat, ΔH:

$$H = h + \Delta H \tag{9}$$

Where

$$h = h_{ref} + \int_{T_{ref}}^{T} c_p dT \tag{10}$$

And h_{ref} = reference enthalpy

T_{ref} = reference temperature

c_p = specific heat capacity at constant pressure

The liquid fraction, β, can be defined as:

$$\beta = 0, \text{if } T < T_{solidus}$$

$$\beta = \text{if } T > T_{liquidus}$$

$$\beta = \frac{T - T_{solidus}}{T_{liquidus} - T_{solidus}} \; if \; T_{solidus} < T < T_{liquidus} \tag{11}$$

The latent heat content can now be written in terms of the latent heat of the material, L:

$$\Delta H = \beta L \tag{12}$$

For solidification/melting problems, the energy equation is written as:

$$\frac{\partial(\rho H)}{\partial t} + \nabla.(\rho \vec{v} H) = \nabla.(k \nabla T) + S \tag{13}$$

Where $\rho = density$

$H = enthalpy$

$\vec{v} = fluid \; velocity$

$S = source \; term$

The solution for temperature is essentially an iteration between the energy equation (13) and the liquid fraction equation (11).

Momentum Equations: The enthalpy-porosity technique treats the mushy region (partially solidified region) as a porous medium. The porosity in each cell is set equal to the liquid fraction in that cell. In fully solidified regions, the porosity is equal to zero, which extinguishes the velocities in these regions. The momentum sink due to the reduced porosity in the mushy zone takes the following form:

$$S = \frac{(1-\beta)^2}{(\beta^3 + \epsilon)} A_{mush}(\vec{v} - \vec{v}_p) \tag{14}$$

where β is the liquid volume fraction, ϵ is a small number (0.001) to prevent division by zero, A_{mush} is the mushy zone constant, and $\vec{v}_p$ is the solid velocity due to the pulling of solidified material out of the domain (also referred to as the pull velocity).

The mushy zone constant measures the amplitude of the damping; the higher this value, the steeper the transition of the velocity of the material to zero as it solidifies. Very large values may cause the solution to oscillate.

The solution methods used were second order upwind scheme to solve the momentum and energy equations, SIMPLE method for pressure–velocity coupling and the PRESTO scheme is adopted for the pressure correction equation. The relaxation factors were used the default setting for the pressure, momentum ,energy, body forces, density and liquid fraction as 0.3, 0.7, 1, 1, 1 and 0.9, respectively.

3.6   Methods in optimization

Design-Expert 11 software, was used to generate the Central Composite Designs. For 2 input parameters (length and thickness), 9 design points are required to build a response surface using the CCD [20].

$\alpha = 1$, is chosen to a suitable value for this analysis. The levels of factors used in this analysis are given in table 12. These levels are chosen based on the value of α. Thus, the CCD design becomes a face-centered composite design with the design points.

Table 7. Design of experiments

DoE type	Central composite design (CCD)					
Input Parameters	type	Range (Design space)				
		Lower bound	Upper bound	levels		
Length (mm)	continuous	70	140	70	105	140
Thickness (mm)	continuous	0.8	1.5	0.8	1.0	1.5

The responses in the optimization process are full solidification time and maximum energy storage capacity, where time response has to be minimized and energy storage capacity has to be maximized. To study the maximum energy storage capacity quantitatively, this parameter is defined as the sum of sensible and latent heat over the entire domain at the beginning of the solidification process.

Thus the energy released is calculated as:

$$Total\ heat\ capcity_{PCM} = sensible\ heat_{PCM} + Latent\ heat_{PCM}$$

$$E\ (kJ) = m_{PCM}C_p(T_i - T_m) + m_{PCM}h_{fl} \tag{15}$$

Mass of PCM is calculated as, $m_{PCM} = \rho_{PCM}V_{PCM}$

Mass of fin is, $m_{fin} = \rho_{Al}V_{fin}$

Volume of PCM, $V_{PCM} = V_{total} - V_{fin}$

Volume of fin, $V_{fin} = thickness * length * width$

Volume of the cylinder, $V_{total} = \pi r^2 H = 0.0045 m^3$

T_i is the temperature of the molten PCM at initial time which is 500 K.

T_m is the melting temperature of PCM which is 415 K.

Table 7, shows the input and the response parameters for the desired optimization.

4 Thermal Load Analysis and Components Design

4.1 Estimation of irradiance on horizontal surface

The operation of solar collectors and systems depends on the solar radiation input and the ambient air temperature and their sequences. This is because, the size of collectors used in the solar applications is based on the available solar radiation on that location. And also it helps designers to quantify cost of materials.

In the area of solar irradiation, there are two common terms used. i.e extraterrestrial and terrestrial solar radiation. Extraterrestrial radiation is the solar radiation incident outside of earth's atmosphere or without considering the atmosphere where as the terrestrial radiation is the solar irradiation on the surface of the earth which includes the beam and diffuse solar irradiation.

Solar irradiation is the amount of available solar energy on the ground surface over a specified time, expressed as kWh/m^2 or MJ/m^2. The sum of direct and diffuse solar irradiation is called global irradiation. The most common model used to estimate monthly average daily solar radiation on horizontal surface is the modified form of the Angstrom-type equation.

$$\frac{H}{H_O} = a + b\left(\frac{n}{N}\right) \tag{16}$$

where H is the monthly average daily global radiation, Ho is the monthly average daily extraterrestrial radiation, n is the day length, N is the maximum possible sunshine duration, and a and b are empirical coefficients [13].

The values of the monthly average daily extraterrestrial radiation (Ho) are calculated for days giving average of each month. Ho in (J/day.m^2) is calculated using the following equation (17).

$$H_o = \frac{24 * 3600 * G_{sc}}{\pi}\left[1 + 0.033\cos\left(\frac{360n}{365}\right)\right] * \left[cos\emptyset cos\delta sin\omega_s + \left(\frac{\pi\omega_s}{180}\right)sin\emptyset sin\delta\right] \tag{17}$$

Where G_{sc} is the solar constant (=1367 W m^{-2}), $\emptyset$ is the latitude of the site, δ is the sun declination angle and ω_s is the mean sunset hour angle for the given month.

For n_d is the day of the year, January first n=1 to 365n days, the declination angle (δ)

$$\delta = 23.45^0 sin\left[360^0\left(\frac{284 + n_d}{365}\right)\right] \tag{18}$$

The sunset hour angle (ω_s) in degrees is calculated as:

$$\omega_s = cos^{-1}(-tan\phi tan\delta) \tag{19}$$

The maximum possible daily hours of bright sunshine (N) is:

$$N = \frac{2 * \omega_s}{15^0} \tag{20}$$

The regression coefficients "a" and "b" are expected to improve by adding the effect of elevation, sunshine duration, and latitude together. Therefore, the regression coefficients "a" and "b" in terms of latitude, elevation and percentage of possible sunshine for any location around the world (for $5° < \emptyset < 54°$) are related with Gopinathan equation [35].

Gopinathan [36] obtained a model which is considered as the most accurate model for estimation of H and the coefficients are:

$$a = -0.309 + 0.539cos\phi - 0.0693\, Z + 0.29\left(\frac{n}{N}\right) \tag{21}$$

$$b = 1.527 - 1.027cos\phi + 0.0926Z - 0.359\left(\frac{n}{N}\right) \tag{22}$$

Where Z is elevation above sea level or altitude in kilometers.

For Jimma elevation, Z = 1780m = 1.78km and altitude angle, $\phi = 7.67°$

Table 8. Recommended Average Days for Months and Values of n_d by Months

Month	n_d for i^{th} day	For the average day of the month		
		Date	Day of the year(n_d)	Declination (δ)
January	i	17	17	-20.9
February	31+i	16	47	-13.0
March	59+i	16	75	-2.4
April	90+i	15	105	9.4
May	120+i	15	135	18.8
June	151+i	11	162	23.1

July	181+i	17	198	21.2
August	212+i	16	228	13.5
September	243+i	15	258	2.2
October	273+i	15	288	-9.6
November	304+i	14	318	-18.9
December	334+i	10	344	-23.0

For long term use as in the design of solar collectors, the solar data has to be studied over months and years. The average numbers of sunshine hour for Jimma were obtained from the daily measurements data taken from national meteorology statistical agency. The sunshine hour data (Appendix B, Table 3) is calculated for 5 years period from 2013 to 2017.
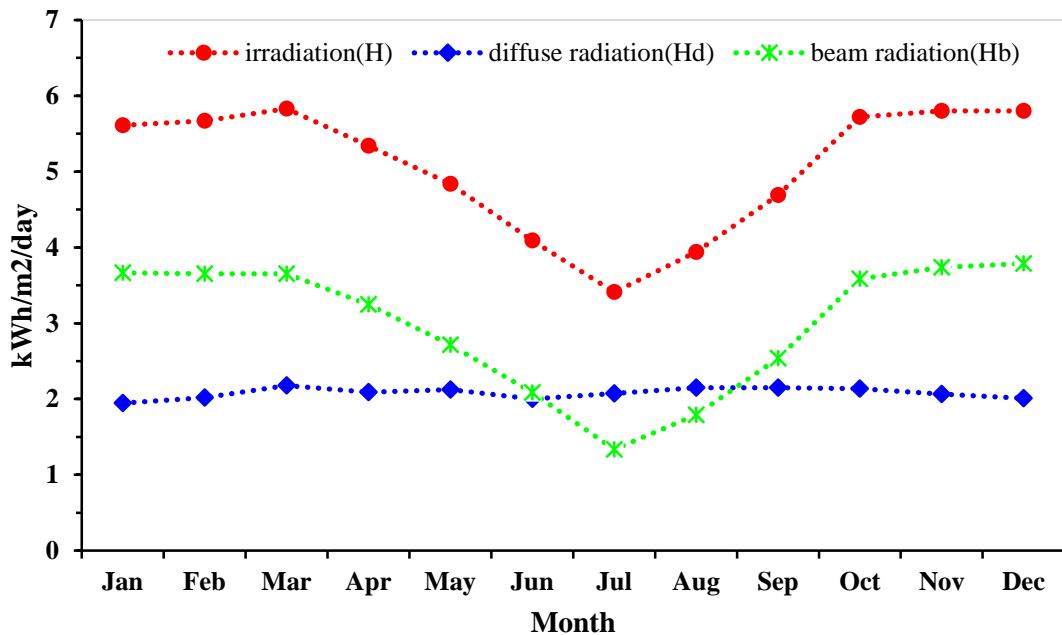

Figure 21. Monthly average of total, diffuse and beam radiation of Jimma from 2013 to 2017

The average annual solar radiation potential of the study area (Jimma) was found to be 5.06 kWh/m^2/day or 788.16 W/m^2 as shown in (Appendix B, Table 4).

Where 1 kWh/m^2/day = 3.6 MJ/m^2

The data in (Appendix B, Table 4) is the total irradiance for horizontal surface and it is important to consider the beam and diffuse radiation in the design of parabolic trough solar collector since the beam radiation is the useful part in these collectors.

The three radiations are related as given in equation (23) and to determine the beam radiation, the diffuse radiation has to be estimated from the clearness index (K_T) for the study area.

$$H_{total} = H_{beam} + H_{diffuse} \tag{23}$$

According to Erbs et al. [37] correlations has developed for monthly average diffuse fraction from the daily diffuse correlations. Jimma which has sunset hour angle (ω_s) that is above 85 degrees for all months is given by equation (24).

For $\omega_s > 81.4^0$ and $0.3 \leq \overline{K}_T \leq 0.8$

$$\frac{\overline{H}_d}{\overline{H}} = 1.311 - 3.022\overline{K}_T + 3.427\overline{K}_T{}^2 - 1.821\overline{K}_T{}^3 \tag{24}$$

After performing the calculations, the average monthly beam radiation, neglecting June and July for the reason that they have cloudy days (399.09 and $390.75 \, ^W/_{m^2}$ respectively) is $470.53 \, ^W/_{m^2}$.

4.2 Energy Requirement for cooking

The heat required for cooking wet (Ethiopian or Eritrean stew) can be defined as the energy required for water and ingredients to raise their temperature from room temperature to the boiling point of water which is called sensible heat and the energy required for evaporation which is called the latent heat. The heat capacity of wet is assumed the same as of the water to reduce complexity in design.

From the collected data, both "misr" and "shiro" were the most repetitive meals for lunch and dinner. For cooking a one-time meal, a family member with 5 people uses an average of 1 liter water and 0.2 Kg of misr or shiro. The amount of water lost during cooking for solar cookers is assumed as 10% of the total water required for cooking [3].

Therefore, the heat required for cooking per kg is:

$$Q = m_w * C_{pw} * (T_{boil} - T_{room}) + m_{vap} * h_{fg} \qquad (25)$$

Where:

m_w − mass of meal = 1.2 kg

C_{pw} − specific heat capacity of water = 4.187 kJ/kg. K

T_{boil} − boiling temperature of water in Jimma = 95°C

T_{room} − room temperature in Jimma = 25 °C

m_{vap} − mass of water lost in vaporization = 0.1 ∗ m_w = 0.12 kg

h_{fg} − heat of vaporization of water = 2260 kJ/kg

Thus:

$$Q = 1.2 \text{ kg} * 4.187 \text{ kJ/kg. K} * (95 - 25)K + 0.12 * 2260\text{kJ/kg}$$

$$= 351.708 + 271.2$$

$$Q = 622.91\text{kJ}$$

During cooking there will be energy loss by means of convection and radiation other than the useful energy spent on the cooking. And for this reason, considering 80% efficiency [4], the total heat required will be:

$$Q = 1.2 * 622.91\text{kJ} = 747.49 \text{ kJ}$$

The system accomplishes two simultaneous processes while operating. It is able to cook during day time and also charge the energy storage for later use. By considering cooking time of 40 minutes, the power required for cooking will be:

$$Power = \frac{heat \; required \; in \; (kJ)}{cooking \; time(s)} = \frac{Q}{t} \qquad (26)$$

The power required for cooking is therefore found to be 0.3115 kW or 311.5 watts.

In order to store energy while cooking, the solar energy delivered by the concentrator must be twice of the calculated energy demand. For this reason the total energy required will be 623 watts.

Adjusting the flow rate is the controlling mechanism for the energy delivered. In the case of charging without cooking, the flow rate will be reduced by half and also insulating the pan seat so as to prevent heat loss.

4.3 PCM storage sizing

In this section the mass of PCM, volume of tank that contains the PCM are to be determined.

The thermo-physical properties of the selected PCM material are shown in table 9.

Table 9. Thermo-physical properties of HITEC salt

Compound	Mass Ratio	Melting Point, ℃	Melting Enthalpy, kJ/kg	Specific Heat J/(kg.K)		Thermal conductivity, W/(m.K)		Density, kg/m³
				Solid	Liquid	Solid	Liquid	
KNO3-NaNO3-NaNO2	53-6-41	142	110	1170	1730	0.720	0.570	2006

4.3.1 Determining mass of PCM

The total mass of PCM required for energy storage is calculated by considering the amount of heat required for cooking as determined above which is 747.49 kJ and latent heat of the storage medium (Hitec molten salt) which is 110 kJ/kg.

Therefore, Mass of storage medium required for supplying desired amount of heat is:

$$m = \frac{Q}{h_{fg}} \tag{27}$$

$$m = \frac{747.49 \ kJ}{110 \ kJ/kg} = 6.795 \ kg$$

Approximating to the next higher value, 7 kg of PCM can considered.

4.3.2 Determination of total volume of storage tank

The volume that can be occupied by the PCM salt is calculated as:

$$Volume \ (V) = \frac{mass \ of \ PCM}{density \ of \ PCM} = \frac{m}{\rho} \tag{28}$$

$$V = \frac{7\ kg}{2006\ kg/m^3} = 0.003489 m^3$$

Where,

Mass of PCM is 7 kg and density of the storage material is given as in table 9, to be $2006\ kg/m^3$.

Now, taking into account that the thermal expansion of PCM and the thermal degradation, it can be assumed that the volume that can be occupied by PCM after melt to be 30 percent increase. Then the new volume is calculated as.

$$volume = 1.3 * 0.003489 m^3 = 0.004536\ m^3$$

For suitable cooking vessel seat the diameter of the cylindrical storage tank is considered as 200 mm or 0.20 m. From the volume of PCM calculated above and diameter of the tank, without considering the volume of fins, the height of the tank (H) can be determined from:

$$\text{Volume of cylinder} = \pi * r^2 * H \qquad (29)$$

$$H = \frac{V}{\pi r^2} = \frac{0.004536\ m^3}{\pi(0.10\ m)^2} = 0.145\ m\ 0r\ 145\ mm$$

4.4   Solar collector sizing

4.4.1 Parabolic trough Geometry

For parabolic trough concentrators it is important to analyze the geometric relation of the theoretical images created by the concentrator.

The shape of a parabola is given by the equation $y^2 = 4fx$ where f is the focal length (the distance from the focal point to the vertex). a is the aperture length of the trough and ϕ_r is the rim angle, the angle from vertical axis to the rim of the trough as shown in figure 22.
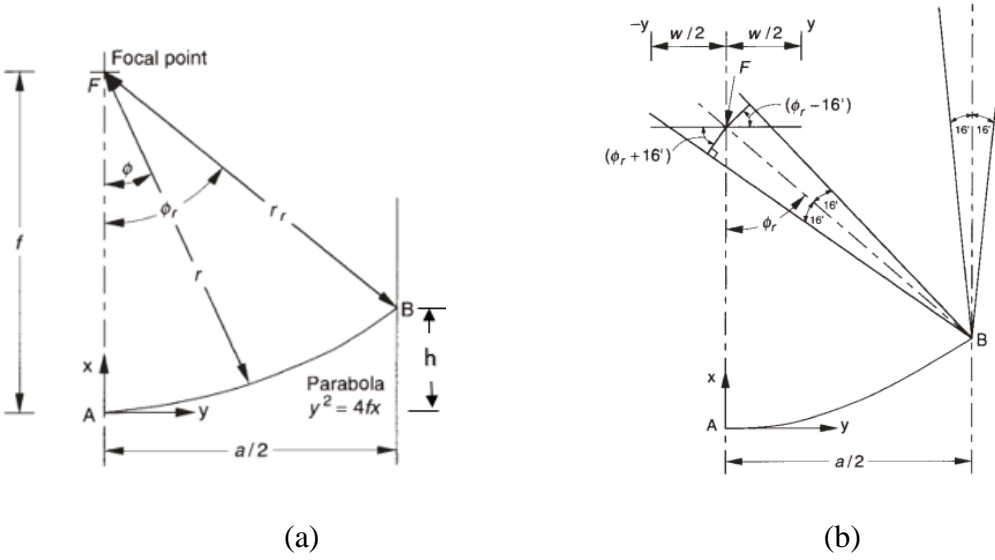
Figure 22. Section of a linear parabolic concentrator (a) and image dimension for a parabolic trough (b) [38][39]

From the equation of a parabola given the height of the parabolic trough, in terms of focal length and aperture diameter is expressed as:

$$\left(\frac{a}{2}\right)^2 = 4fh \qquad or$$

$$h = \frac{a^2}{16f} \tag{30}$$

The focal length can also be related with the rim angle and the aperture diameter as:

$$\tan\frac{\phi_r}{2} = \frac{a}{4f} \tag{31}$$

4.4.2 Concentration ratio (C)

Another important parameter in solar concentrators is the concentration ratio which is defined as the ratio of the aperture area of collector (A_c) to area of absorber/receiver (A_r).

$$C = \frac{A_c}{A_r} \tag{32}$$

4.4.3 Absorber sizing

For maximum geometric concentration ratio, the optimal trough rim angle is $\phi r = 90°$ [4]. For specular parabolic reflectors of perfect shape and alignment, the size of the receiver to intercept all of the solar image can be calculated. The diameter D of a cylindrical receiver is given as:

$$D = r_r \sin 0.267 = \frac{a \sin 0.267}{\sin \phi_r} \tag{33}$$

According to the specified geometric dimensions and relations an absorber tube with a diameter D of 4.6 mm is theoretically necessary to collect the sun rays under perfect conditions, considering a solar angle of 0.267 deg. For this study, a diameter of 20 mm is chosen for good balance between optimal collection (tolerating tracking inaccuracy), sufficient concentration ratio and availability of materials [39].

The estimated rate of useful energy absorbed by the food from the PTC is given by [38]:

$$\dot{Q}_u = \eta_{th} I_b A_a \tag{34}$$

The efficiency range of most solar concentrators is 40%-60% [38]. The solar beam radiation intensity of study area as estimated is 470.53 w/m2.

Considering, $\eta_{th} = 0.5$ (average of 0.4 and 0.6), the aperture area of the parabolic trough collector can be calculated as:

$$A_c = A_a = \frac{\dot{Q}}{\eta_{th} I_b} \tag{35}$$

The area of the parabolic trough collector (A_a) is therefore calculated as 2.65 m². Since, the aperture length has previously specified to be 1 m, then the length of the collector is 2.65 m.

Selected receiver tube is Copper tube with 20 mm inner diameter and 22 mm outer diameter.

Area of receiver, $A = \pi DL$

Area of receiver exposed to rays (Ar) is:

$$A_r = \frac{\pi DL}{2} = \frac{\pi * 0.022 * 2.65}{2} = 0.092 \, m2$$

Arc length: Another property of the parabola that may use in understanding solar concentrator design is the arc length (s).

$$S = \left(\frac{D}{2}\right)\sqrt{\left(\frac{4h}{D}\right)^2 + 1} + 2fln\left(\frac{4h}{D} + \sqrt{\left(\frac{4h}{D}\right)^2 + 1}\right) \tag{36}$$

Table 10. Geometrical specifications and calculated values of parabolic trough collector

Description	symbol	Value
Aperture	a	1 m
Length	L	2.65 m
Rim angle	ϕ_r	90 degrees
Focal length	f	0.25 m
Arc length	S	1.148 m
Concentrator height	h	0.25 m
Receiver diameter	D_r	22 mm
Aperture area	A_C	2.65 m^2
Receiver area	A_r	0.092 m^2
Geometric C.R	C.R	28.9

4.4.4 System thermal performance

In analyzing solar collectors, not all the incident solar radiation onto the concentrator surface is intercepted and captured by the absorber or receiver. There will be heat loss to the environment by radiation, convection and by conduction in the supporting structure. Neglecting conduction heat loss, the Convective and radiation losses from receiver are computed as:

$$\dot{Q}_{conv,loss} = h_c A_r (T_r - T_a) \tag{37}$$

$$\dot{Q}_{rad,loss} = \varepsilon\sigma A_r (T_r^4 - T_a^4) \tag{38}$$

Concerning the losses by convection, the convective coefficient h_c is deduced from the Reynolds and Nusselt numbers [40].

$$Re = \frac{vL}{v} \tag{39}$$

$$Nu = \frac{h_c L}{k} \tag{40}$$

The combined heat loss will be the sum of the convective and radiation loss.

$$\dot{Q}_L = \dot{Q}_{loss} = h_c A_r (T_r - T_a) + \varepsilon \sigma A_r (T_r{}^4 - T_a{}^4) \tag{41}$$

Therefore, the total heat rate on the receiver is the sum of the useful energy transported by the fluid and the losses. This can be expressed as:

$$\dot{Q}_R = \dot{Q}_U + \dot{Q}_L \tag{42}$$

Where:

$\dot{Q}_R$ is energy on receiver

$\dot{Q}_U$ is useful enrgy and

$\dot{Q}_L$ is heat loss from receiver

From these relations, the useful energy is:

$$\dot{Q}_U = \dot{Q}_R - \dot{Q}_L \tag{43}$$

5 Results and Discussions

5.1 Introduction

In this section the CFD results of the fin assisted thermal storage, the design optimization using response surface method and the validation of the optimized design with experimental results are presented and discussed.

The melting and solidification processes were numerically modelled using commercial CFD software ANSYS Fluent 16.0.

5.2 The effect of fin parameters on PCM melting rate

Figure 23, shows the effects of fin thickness on the thermal response of the storage system with time during the charging process. The numbers of fins used were eight, reducing them in to four by using symmetry in the numerical model. The length of fins was constant and 140 mm which is the longest among (70, 105 and 140 mm).

During melting, natural convection dominates the heat transfer process. A high number of fins could be restrict the motion of molten the PCM which can result in a strong suppression of the natural convection. Increasing the length of the fins will allow high thermal penetration which results high heat-transfer from the hot walls of the fin the PCM.

The completion time of the melting process was 4.16, 3.62 and 2.78 hr. for the fin thicknesses of 0.8, 1 and 1.5 mm respectively. The PCM is initially at 300 K temperature before supplying heat. The temperature then increases up to the interrupted region of the curves shown in figure 23 where the phase change occurs at a constant temperature of 415 K. The energy storing/ melting rate and temperature has increased with increasing the fin thickness. The 1.5 mm and 1 mm thick fins show 49.6% and 30.2% melting rate enhancement in comparison with 0.8 mm thick fin respectively.
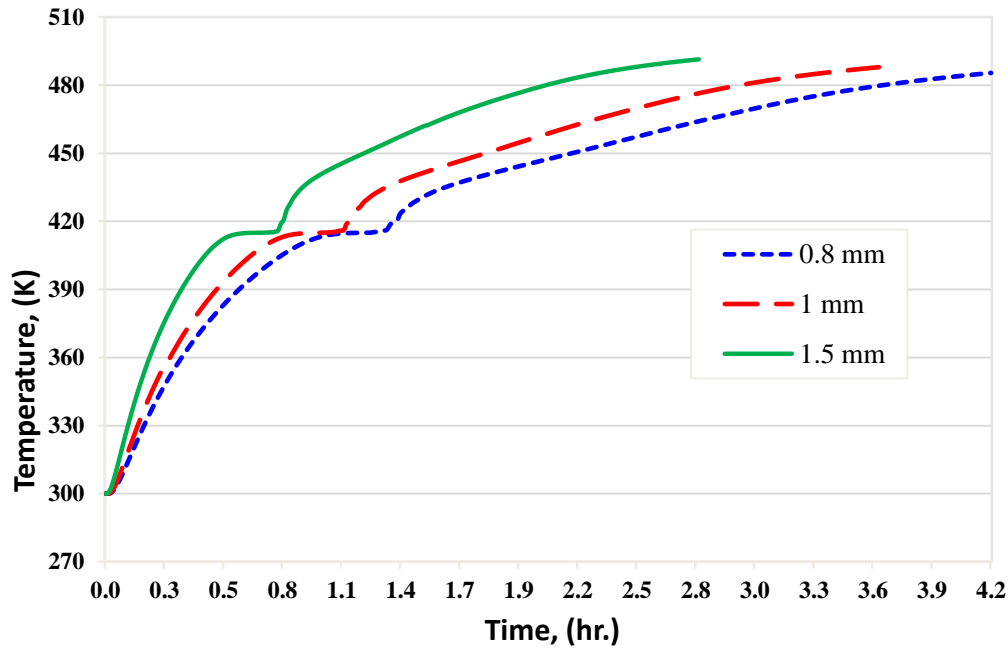
Figure 23. PCM temperature history during melting

The liquid fraction variation with time for the three fin thicknesses is also shown in figure 24. Which follows similar pattern with the temperature profile. Zero value of the liquid fraction shows, the PCM is in solid state. During the phase transformation it lies in between zero and one. When the liquid fraction attains a value of one it is in molten PCM.
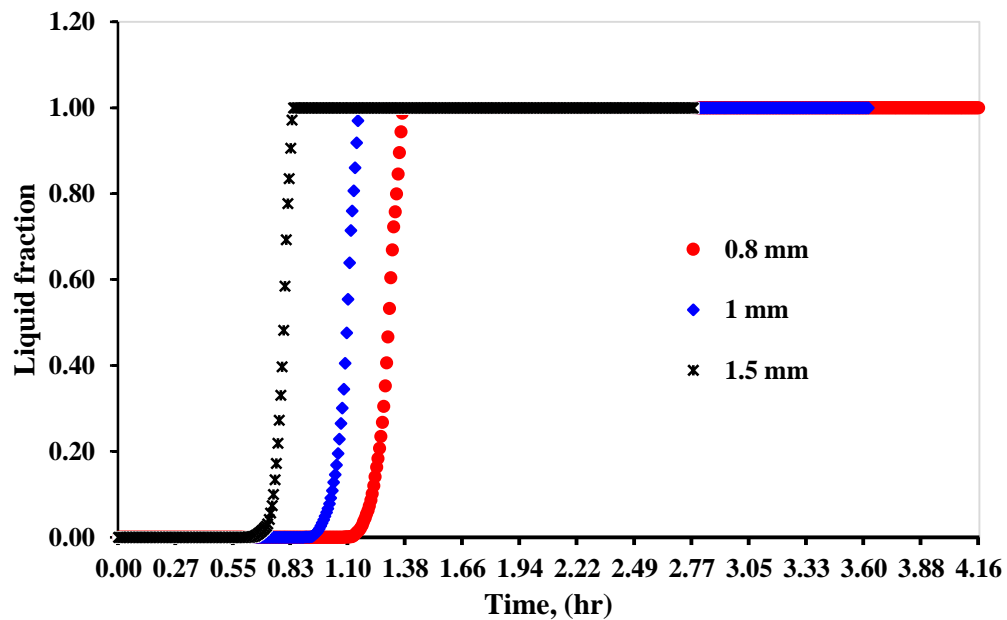

Figure 24. Liquid fraction variation with time

5.3   The effect of fin parameters on solidification rate

The present study investigates the effect of using different parameters of aluminum fins for solidification enhancement of the PCM. The effect of the fins' was studied by benchmarking the performance of the storage with a case if fins were not used.

Figure 25, shows liquid fraction contours of a PCM without immersing fins and with fins of various thicknesses in effect for the solidification rate. The fins dimensions were 0.8, 1 and 1.5 mm thick and with same length of 140 mm. the solidification time was 10.24, 9.75 and 8.9 hours for 0.8, 1 and 1.5 mm fins respectively. The solidification time of PCM was reduced as the thickness has increased. Initially the presence of the fin doesn't have better contribution for the solidification but later on the, when the top part is solidified, the fins use as heat pipe which guides thermal penetration from inside out.

7.0 hr				
8.5 hr				
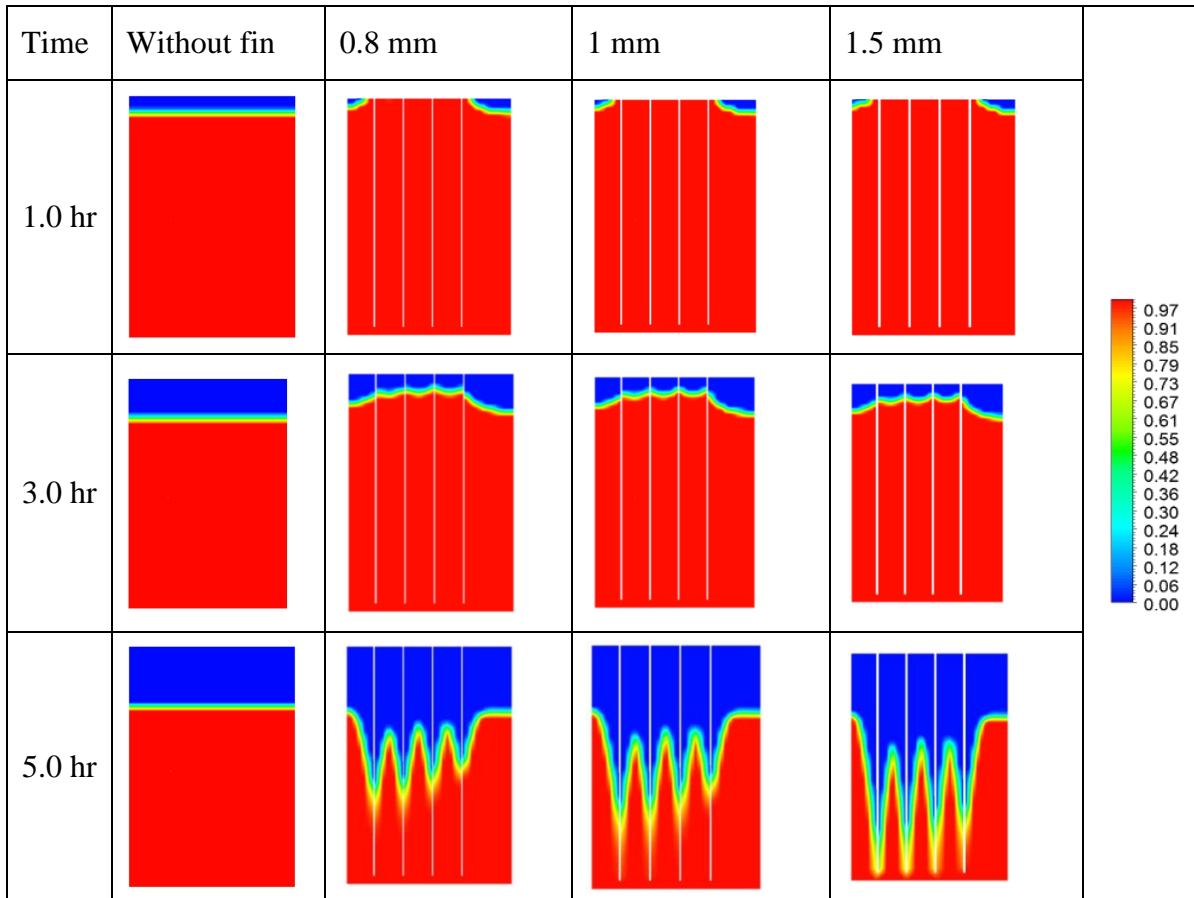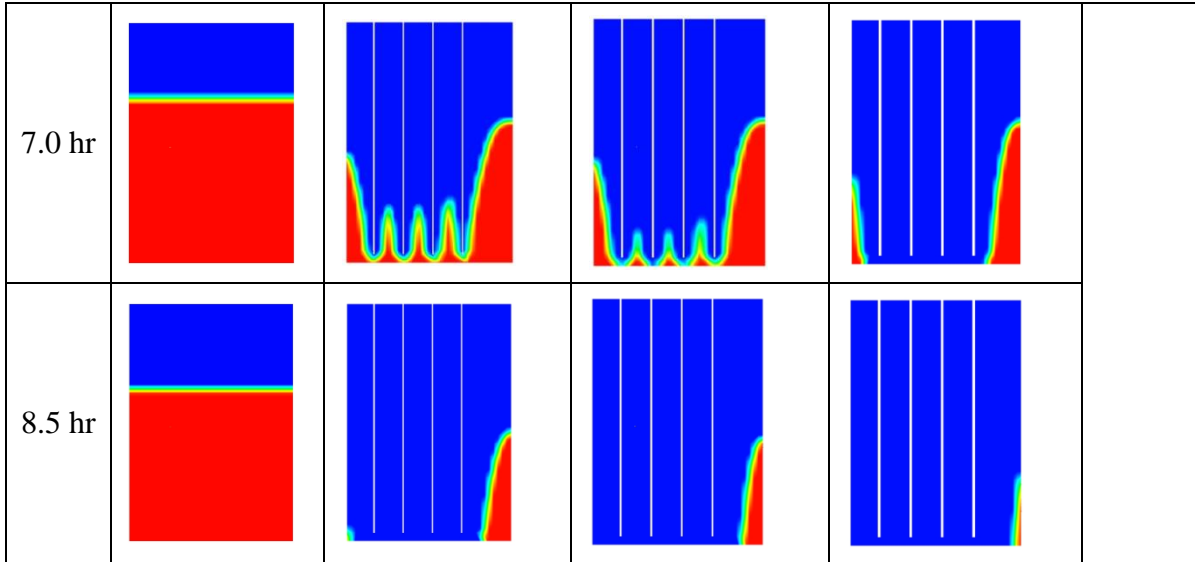
Figure 25. Liquid fraction contours of PCM without fin, and with different fin thickness and same length.

The PCM is first in molten state that initially natural convection can have significant role but later the solidification process is dominated by conduction. In the simulation, natural convection has been neglected but the experimental result shows the fin with small thickness has performed well at initial stage of the solidification process. The numerical and experimental temperature history are shown in figure 26.
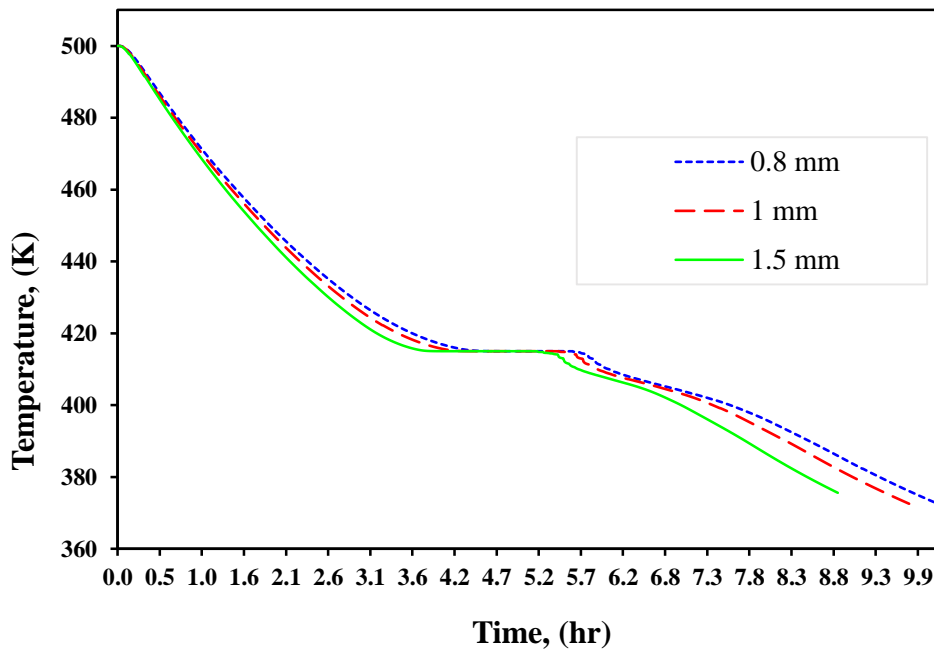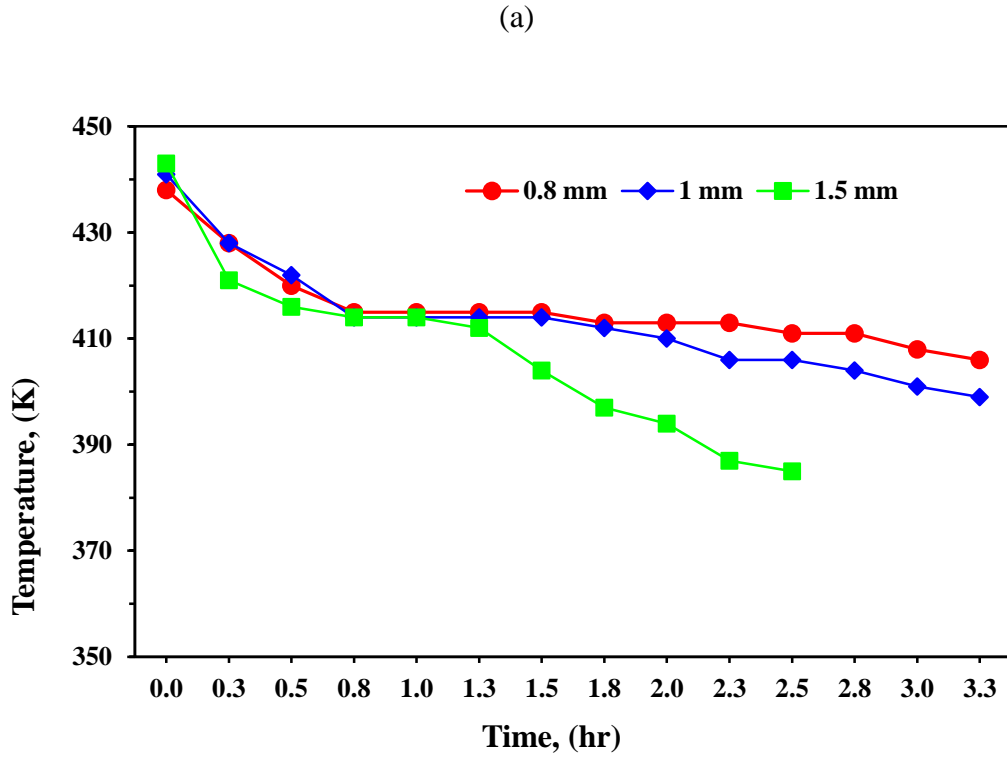
Figure 26. Variation of temperature with time during solidification, numerical (a) and experimental (b).

The effect of fin length on solidification rate with the contours of liquid fraction and temperature distribution is presented on figure 27 and 28.

The long fins provide high interfacial surface area between the PCM and the surface of fins. This allows the heat transfer from the PCM to the fins more facilitated as the fin has more temperature gradient being immersed on the solidified and liquid region of the PCM. This also has the advantage of providing uniformed temperature distribution within the PCM.

Figure 27. Liquid fraction contours of PCM with different fin lengths and same thickness.
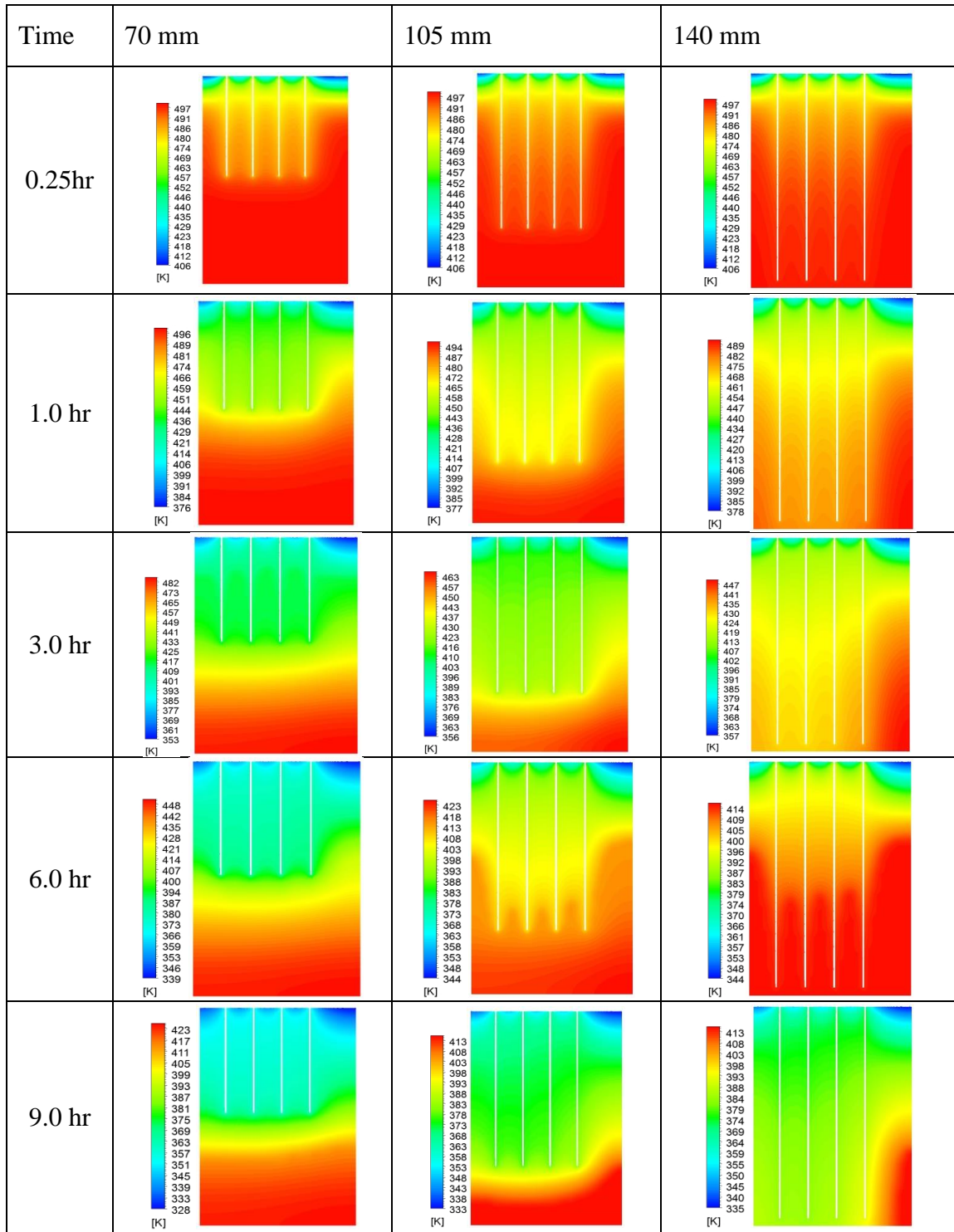
Figure 28. Temperature contours of PCM with different fin lengths and same thickness.

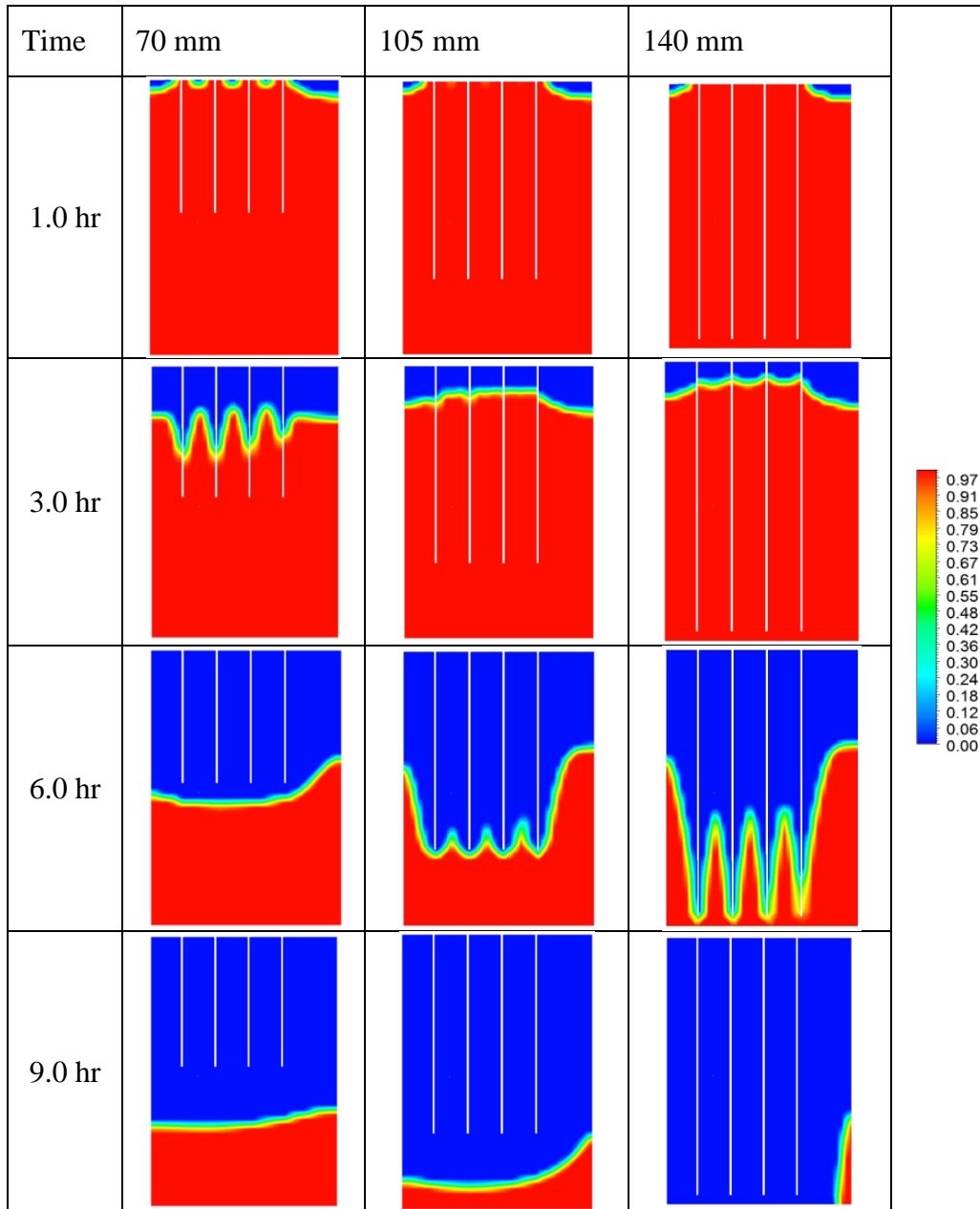In general, table 11, shows the time required for complete solidification with various fin design parameters on PCM and without fin for comparisons. The table presents the percent reduction in time required for solidification in all by comparing with the finless PCM storage. It can be seen that the shorter length of fins affects the solidification rate much more than the thickness. On contrary, the better performance was achieved by using the longest fins. Using the fin with thickness of 1.5 mm and length of 140 mm can reduce solidification rate by 65.97% than without using fins, which greatly enhances the heat transfer rate.

Table 11. Required time for the complete solidification and the time reduction percentage for all fins and PCM without fins.

Thickness (mm)	Length (mm)	Solidification time (hr.)	Reduction in time (%)
0.8	70	15.53	40.63
0.8	105	12.10	53.74
0.8	140	10.24	60.85
1	70	15.22	41.82
1	105	11.70	55.27
1	140	9.75	62.73
1.5	70	14.65	43.9
1.5	105	10.95	58.14
1.5	140	8.90	65.97
Without fin		26.16	-

The CFD and Experimental results has been compared and both are in good agreement that the CFD could be used as design tool. Figure 29, represents the temperature profile of a PCM for both methods. The experimental results show faster rate in solidification process due to the reason that heat has dissipated through the ash insulation of the storage and small gaps on sealings, unlike in the CFD which is completely insulated.
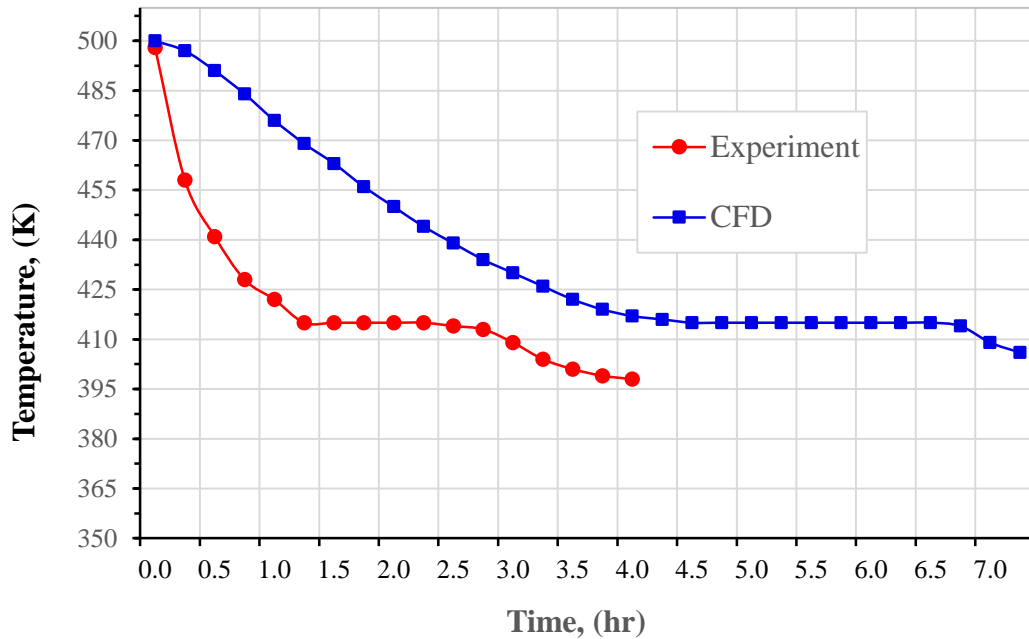
Figure 29. Temperature history of PCM using experiment and CFD methods.

5.4 Temperature distribution on Pan Surface

Figure 30, shows the experimental and CFD result of temperature distribution on the surface of a pan without loading food. It is exposed to natural convection and radiation. The radial temperature distribution is taken at four locations (0, 30, 60 and 90 mm) of the pan. The temperature shows higher towards the center of the pan where the fins are located closer than to the periphery of the cylinder. The space near to the cylindrical container (PCM capsule) is not good enough to accommodate rectangular fins which as a result has reduced temperature value. The graph for temperature of the pan with time shows similar pattern with that of PCM solidification graph, where temperature during the initial hours is high and at the phase change of the PCM the temperature at the pan is maintained to be constant which later drops for sensible solidification. The temperature of the pan needs to heat up at the very beginning of the solidification process as shown in figure 30, with the sharp increasing curve.
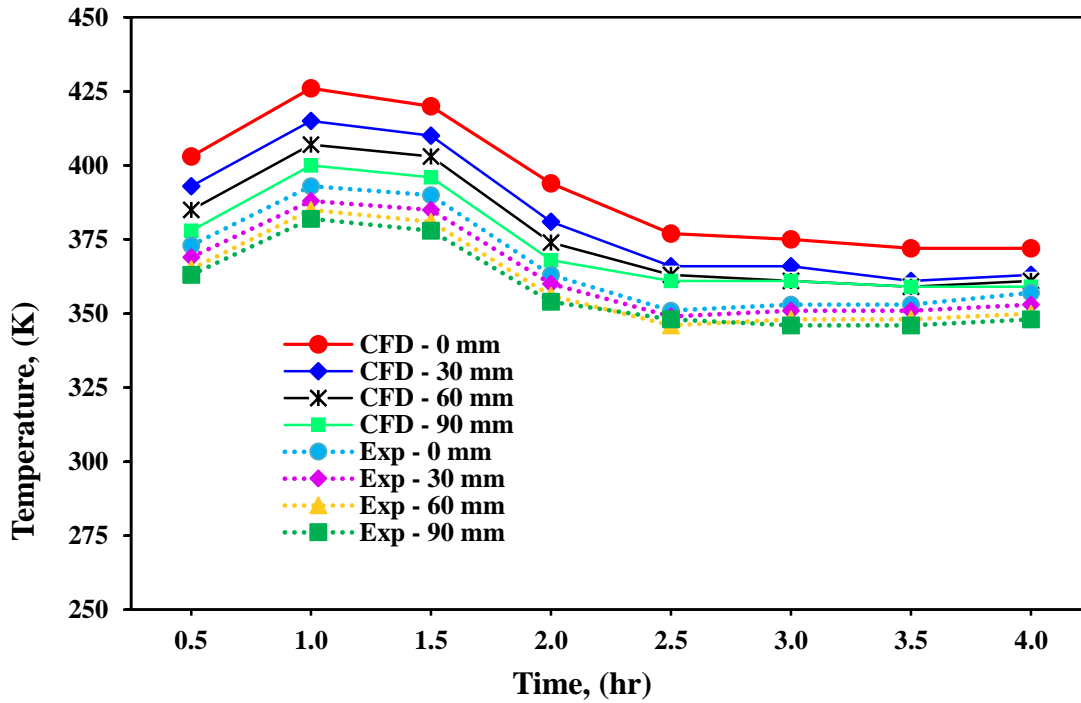
Figure 30. Temperature distribution on different pan locations with time.

The pan performance with the different fin lengths is shown in the CFD model given figure 31. It can be observed that the longest fins provide higher temperatures and faster rate of solidification in comparison with shorter fins.
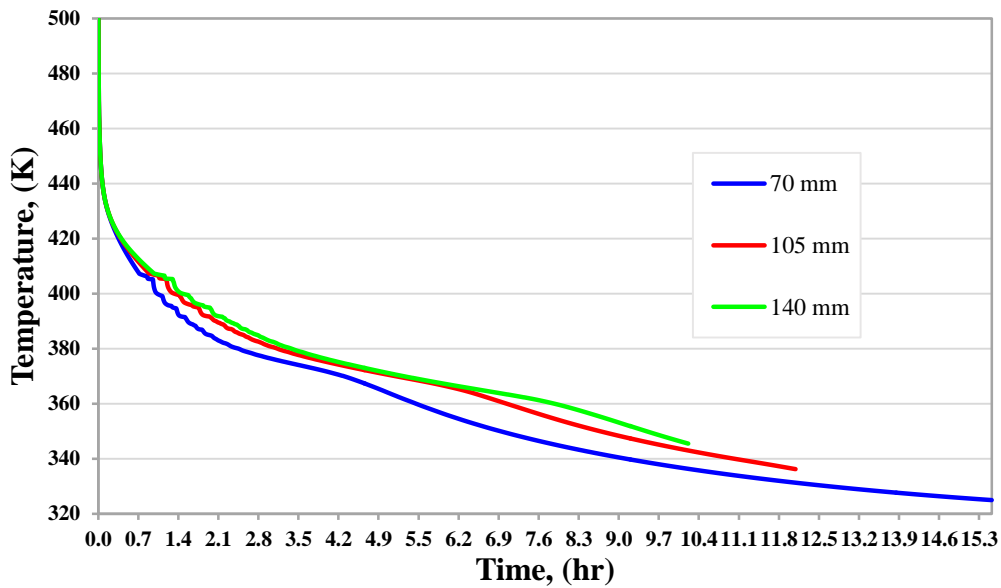
Figure 31. Pan temperature distribution with time for different fin length.

5.5 Design optimization

The Coefficient of Determination (R^2) shows the ratio of the explained variation to the total variation. It normally varies from 0 to 1 and the best value is 1 [34]. In figure 32, the predicted values verses the CFD solidification time and heat capacity is shown and it indicates the quality of response surface and the actual or CFD values. In this model the coefficient of determination are 0.997 and 0.9999 for time and heat capacity analysis which are close enough to unity and this shows that the CFD simulation has good agreement with the predicted one.
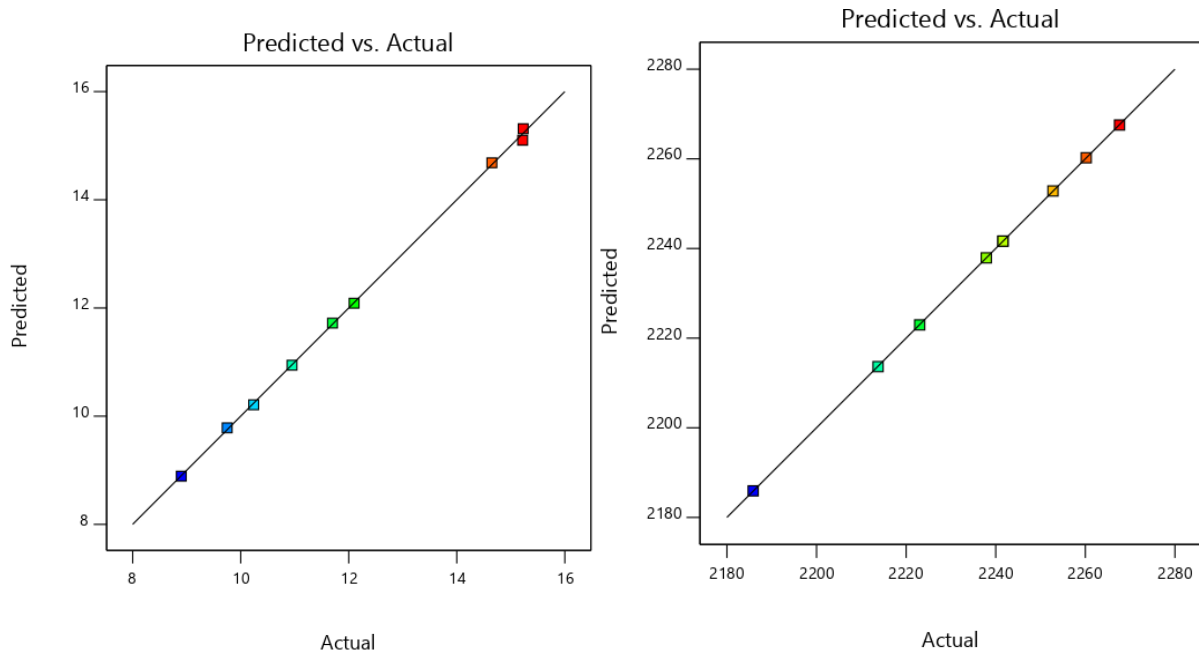
Figure 32. Goodness of fit for time and heat capacity models

Table 12. Central composite designs and results

Thickness (mm)	Length (mm)	Heat Capacity (KJ)	Solidification time (hr.)
0.8	70	2267.64	15.53
0.8	105	2252.77	12.10
0.8	140	2237.91	10.24
1	70	2260.21	15.22
1	105	2241.62	11.70
1	140	2223.04	9.75
1.5	70	2241.62	14.65
1.5	105	2213.75	10.95
1.5	140	2185.87	8.90

Figure 33, (a) and (b) shows the response surfaces of the optimization process. The time for complete solidification is in the range of 8.9 to 15.23 hours for the 9 design points while the total heat capacity is in the range of 2185.87 to 2267.64 kJ. The time is minimum towards the longer and thick fin which is also minimum energy storage. The heat capacity is maximum towards the thin and short fin parameters which is delays solidification time. Figure 33 (c) gives the desirability response surface for the optimum design of minimum time and maximum heat capacity.
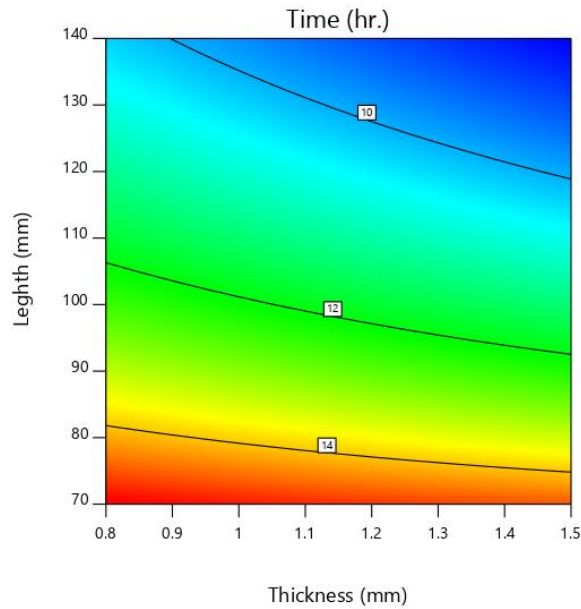
(a)
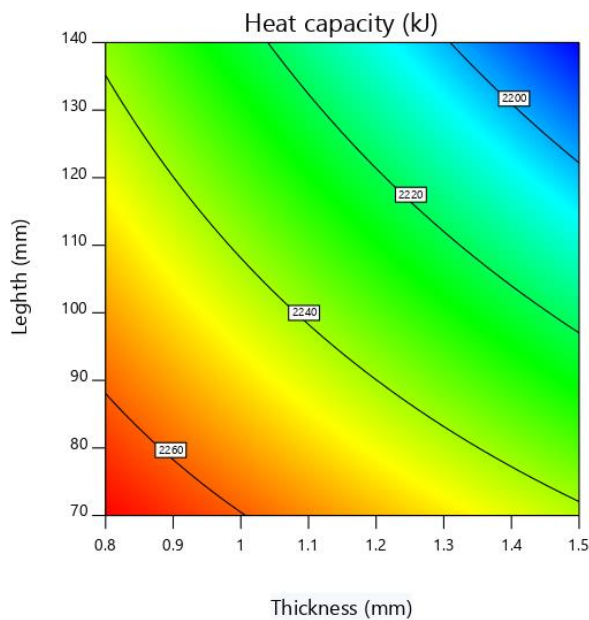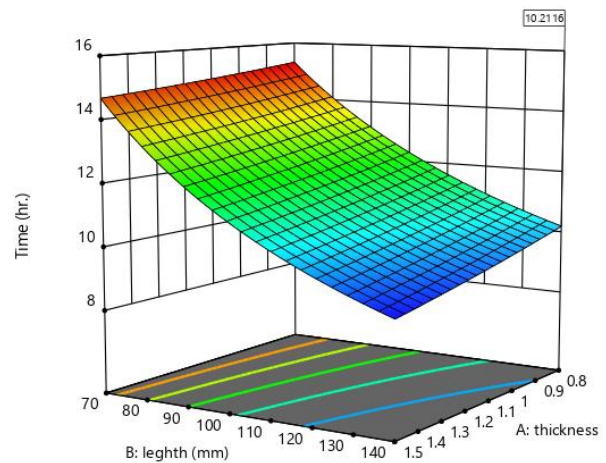
(b)
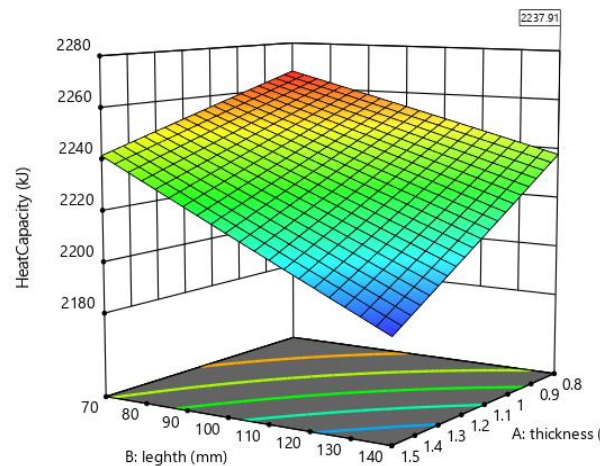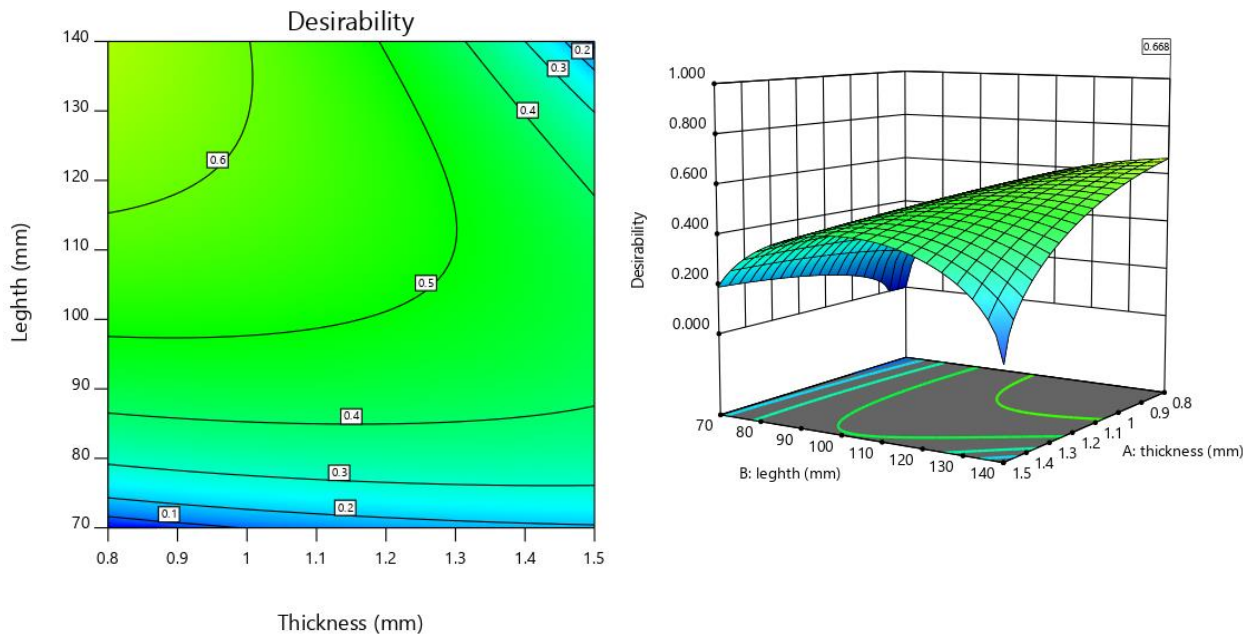
(c)

Figure 33. Full solidification time and total heat capacity response surfaces for fin geometry parameters.

The optimum fin parameter was found to be 0.8 mm thick and 140 mm long fin that yields full solidification time of 10.21 hr. and heat storage capacity of 2237.91 kJ as shown in figure 34.
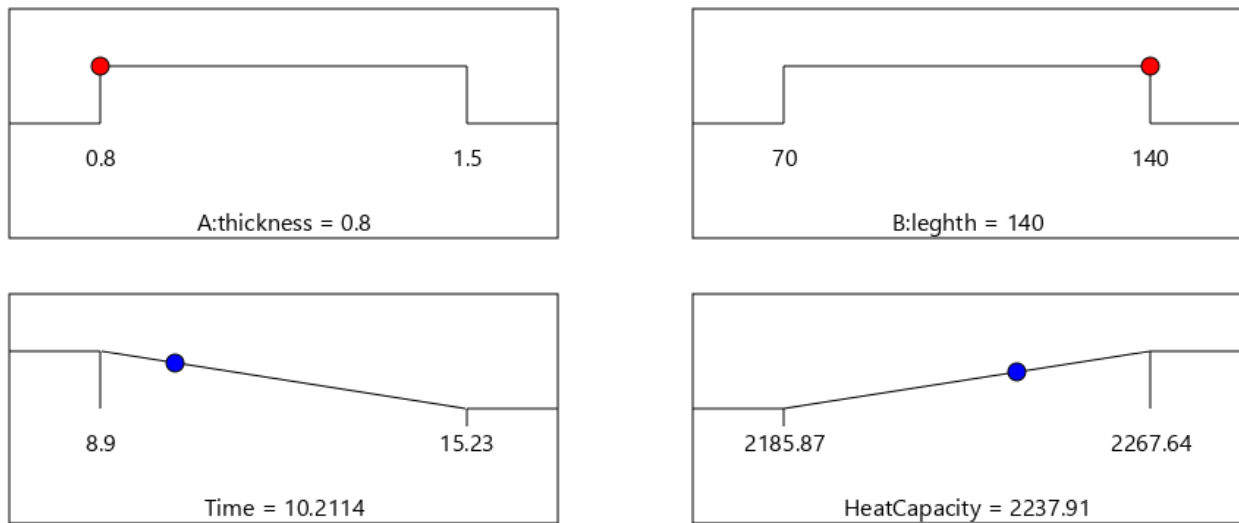
Figure 34. Optimized fin design parameter.

6 Conclusion and Recommendations

6.1 Conclusion

This work presents the use of extended surfaces (fins) for performance enhancement of Phase Change Materials (PCM) as a medium of thermal energy storage in solar cooking application. The study started by exploring different solar collectors and phase change materials which are suitable for cooking.

Thermal loads required for cooking demand are investigated, a parabolic trough solar collector is designed followed by the solar beam assessment of the study area (Jimma) and energy storage is designed. A cylindrical vessel for PCM as latent heat storage and rectangular aluminum fins confinement was built and studied by numerical simulations (computational fluid dynamics, CFD) and experiments.

A 2D numerical melting/solidification models were used in CFD simulation to study the rate of heat transfer during melting and solidification for all design points. In the simulation, the variation of thickness and length parameters of the fin were studied. The length variation has significant effect over the thickness for heat transfer rate. The experiment was used for the solidification process. Both studies yielded good agreements.

Response Surface Method (RSM) was used for design optimization of the heat transfer rate and energy storage capacity of the latent heat storage. Nine design points were generated using central composite. Solidification time was used from the simulations while the heat release/storage capacity was calculated manually considering the mass reduction as it is replaced by fins. From this the fin with thickness of 0.8 mm and length of 140 mm yielded the best design.

6.2   Recommendations

This work has shown that the performance of a latent heat storage system can be enhanced for better design in exploiting solar energy for household cooking application. Furthermore, the following recommendations can be addressed for future research work in the field of thermal energy storage using phase change materials.

- The use of PCM for energy storage can be extended for rural health cares and schools at large scale by increasing the solar harnessing.
- It would also be interesting if the heat transfer enhancement in the cooking area is further studied by using suitable cascaded phase change materials that maximizes the space for the storage material.
- The 2D model CFD simulation can be further studied using 3D model for better results.
- One can study the economic analysis of the complete system.
- The study can be an input for design optimization of waste heat recovery systems with finned PCM.

References

[1]   A. H. Mondal, E. Bryan, C. Ringler, D. Mekonnen, and M. Rosegrant, "Ethiopian energy status and demand scenarios : Prospects to improve energy ef fi ciency and mitigate GHG emissions," *Energy*, vol. 149, pp. 161–172, 2018, doi: 10.1016/j.energy.2018.02.067.

[2]   "No Titl." https://energypedia.info/wiki/Ethiopia_Energy_Situation#Solar_Energy (accessed Sep. 20, 2019).

[3]   "solar GIS map." https://commons.wikimedia.org/wiki/File:SolarGIS-Solar-map-Ethiopia-en.png (accessed Jul. 10, 2019).

[4]   S. Kalaiselvam and R. Parameshwaran, *Thermal Energy Storage Technologies*. .

[5]   A. Sharma, V. V. Tyagi, C. R. Chen, and D. Buddhi, "Review on thermal energy storage with phase change materials and applications," *Renew. Sustain. Energy Rev.*, vol. 13, no. 2, pp. 318–345, 2009, doi: 10.1016/j.rser.2007.10.005.

[6]   L. Nkhonjera, T. Bello-Ochende, G. John, and C. K. King'ondu, "A review of thermal energy storage designs, heat storage materials and cooking performance of solar cookers with heat storage," *Renew. Sustain. Energy Rev.*, vol. 75, no. November 2016, pp. 157–167, 2017, doi: 10.1016/j.rser.2016.10.059.

[7]   N. I. Ibrahim, F. A. Al-sulaiman, S. Rahman, B. S. Yilbas, and Z. Sahin, "Heat transfer enhancement of phase change materials for thermal energy storage applications : A critical review," *Renew. Sustain. Energy Rev.*, vol. 74, no. October 2015, pp. 26–50, 2017, doi: 10.1016/j.rser.2017.01.169.

[8]   S. Jegadheeswaran and S. D. Pohekar, "Performance enhancement in latent heat thermal storage system : A review," vol. 13, pp. 2225–2244, 2009, doi: 10.1016/j.rser.2009.06.024.

[9]   I. Sarbu and A. Dorca, "Review on heat transfer analysis in thermal energy storage using latent heat storage systems and phase change materials," *Int. J. Energy Res.*, vol. 43, no. 1, pp. 29–64, 2019, doi: 10.1002/er.4196.

[10]   A. H. Tesfay, "Experimental Investigation of a Concentrating Solar Fryer with Heat Storage," Norwegian University of Science and Technology (NTNU), Trondheim, 2015.

[11]   "flat plate solar collectors." https://www.e-education.psu.edu/eme811/node/685 (accessed Aug. 12, 2019).

[12]   W. Chamsa-Ard, S. Sukchai, S. Sonsaree, and C. Sirisamphanwong, "Thermal performance testing of heat pipe evacuated tube with compound parabolic concentrating Solar collector BY ISO 9806-1," *Energy Procedia*, vol. 56, no. C, pp. 237–246, 2014, doi: 10.1016/j.egypro.2014.07.154.

[13]   Soteris A. Kalogirou, *Solar Energy Engineering, Processes and Systems*, Second. 2014.

[14]   M. Kenisarin and K. Mahkamov, "Solar energy storage using phase change materials," *Renew. Sustain. Energy Rev.*, vol. 11, no. 9, pp. 1913–1965, 2007, doi: 10.1016/j.rser.2006.05.005.

[15]   I. Sarbu, "Review on heat transfer analysis in thermal energy storage using latent heat storage systems and phase change materials," no. June, pp. 1–36, 2018, doi: 10.1002/er.4196.

[16]   A. Hassan, M. S. Laghari, and Y. Rashid, "Micro-encapsulated phase change materials: A review of encapsulation, safety and thermal characteristics," *Sustain.*, vol. 8, no. 10, 2016, doi: 10.3390/su8101046.

[17]   M. D. Silverman and J. R. Engel, "Survey of Technology for Storage of Thermal Energy in Heat Transfer Salt," p. 32, 1977, doi: 10.2172/7232535.

[18]   P. Sivasamy, A. Devaraju, and S. Harikrishnan, "ScienceDirect Review on Heat Transfer Enhancement of Phase Change Materials (PCMs)," *Mater. Today Proc.*, vol. 5, no. 6, pp. 14423–14431, 2018, doi: 10.1016/j.matpr.2018.03.028.

[19]   R. V. Seeniraj and N. Lakshmi Narasimhan, "Performance enhancement of a solar dynamic LHTS module having both fins and multiple PCMs," *Sol. Energy*, vol. 82, no. 6, pp. 535–542, 2008, doi: 10.1016/j.solener.2007.11.001.

[20]   D. C. Montgomery, *optimization book*. 2020.

[21]   L. K. Sahoo, "SOLAR COOKER WITH LATENT HEAT STORAGE : DESIGN AND EXPERIMENTAL TESTING," vol. 38, no. 5, pp. 493–498, 1997.

[22]   S. D. Sharma, "Thermal performance of a solar cooker based on an evacuated tube solar collector with a PCM storage unit," vol. 78, pp. 416–426, 2005, doi: 10.1016/j.solener.2004.08.001.

[23]   H. H. El Ghetany and S. A. Nada, "Experimental investigation of novel indirect solar cooker with indoor PCM thermal storage and cooking unit," no. August, 2008, doi: 10.1016/j.enconman.2008.01.026.

[24]   R. M. Muthusivagami, R. Velraj, and R. Sethumadhavan, "Solar cookers with and without thermal storage — A review," vol. 14, pp. 691–701, 2010, doi: 10.1016/j.rser.2008.08.018.

[25]   U. Stritih, "An experimental study of enhanced heat transfer in rectangular PCM thermal storage.," *United Kingdom:*, 2004, doi: 10.1016/j.ijheatmasstransfer.2004.02.001.

[26]   S. Mat, A. A. Al-abidi, K. Sopian, M. Y. Sulaiman, and A. Th, "Enhance heat transfer for PCM melting in triplex tube with internal – external fins," *ENERGY Convers. Manag.*, vol. 74, pp. 223–236, 2013, doi: 10.1016/j.enconman.2013.05.003.

[27]   J. M. Mahdi and E. C. Nsofor, "Solidi fi cation enhancement of PCM in a triplex-tube thermal energy storage system with nanoparticles and fi ns," *Appl. Energy*, vol. 211, no. November 2017, pp. 975–986, 2018, doi: 10.1016/j.apenergy.2017.11.082.

[28]   S. Lohrasbi, M. Sheikholeslami, and D. D. Ganji, "Discharging Process Expedition of NEPCM in Fin-assisted Latent Heat Thermal Energy Storage System," *J. Mol. Liq.*, 2016, doi: 10.1016/j.molliq.2016.06.044.

[29]   "Jimma Location Coordinates." https://en.wikipedia.org/wiki/Jimma (accessed Aug. 13,

2019).

[30] R. Hindersah, Z. Handyman, F. N. Indriani, P. Suryatmana, and N. Nurlaeny, "JOURNAL OF DEGRADED AND MINING LANDS MANAGEMENT Azotobacter population, soil nitrogen and groundnut growth in mercury-contaminated tailing inoculated with Azotobacter," *J. Degrad. Min. L. Manag.*, vol. 5, no. 53, pp. 2502–2458, 2018, doi: 10.15243/jdmlm.

[31] "survey." https://www.surveysystem.com/sscalc.htm#one (accessed Aug. 13, 2019).

[32] C. Guo and W. Zhang, "Numerical simulation and parametric study on new type of high temperature latent heat thermal energy storage system," *Energy Convers. Manag.*, vol. 49, no. 5, pp. 919–927, 2008, doi: 10.1016/j.enconman.2007.10.025.

[33] S. Tiari, S. Qiu, and M. Mahdavi, "Discharging process of a finned heat pipe-assisted thermal energy storage system with high temperature phase change material," *Energy Convers. Manag.*, vol. 118, pp. 426–437, 2016, doi: 10.1016/j.enconman.2016.04.025.

[34] J. Epinette and K. Sutton, "Fluent User′s Guide," no. November, pp. 1–44, 2003.

[35] Getnet Zewde Somano and Dr. Ing Getachew Shunki Tibba, "Energy Resource Potential Assessment for Solar Photovoltaic-Micro Hydro Hybrid Power Generation System. (A case study for Jimma, Toli Kerso, Minko Village)," *Int. J. Eng. Res. Technol.*, vol. 5, no. 1, pp. 333–340, 2016.

[36] K. K. Gopinathan, "A general formula for computing the coefficients of the correlation connecting global solar radiation to sunshine duration," *Sol. Energy*, vol. 41, no. 6, pp. 499–502, 1988, doi: 10.1016/0038-092X(88)90052-7.

[37] D. C. Montgomery, *Design and Analysis of Experiments*, Eighth. John Wiley& Sons, Inc.

[38] J. A. Duffie, W. A. Beckman, and J. McGowan, *Solar Engineering of Thermal Processes*, vol. 53, no. 4. 1985.

[39] Z. Sen, *solar energy fundamentals and modelling techniques*. Turkey: springer, 2008.

[40] C. Yunus A and G. Afshin J, *Heat and Mass Transfer*, Fifth. McGraw-Hill Educatio, 2015.

Appendix

Appendix A

Table 1. Experimental data recording format

Date_____

Fin size_____

Thermocouple reading in mv																
Time																
PCM (vertical)																
1																
2																
3																
4																
Pan (radial)																
1																
2																
3																
4																
T_∞																

Table 2. Thermocouple reading conversion table

K°C

Type K Thermocouple — *thermoelectric voltage as a function of temperature (°C); reference junctions at 0 °C*

Thermoelectric Voltage in Millivolts

°C	0	1	2	3	4	5	6	7	8	9	10	°C
0	0.000	0.039	0.079	0.119	0.158	0.198	0.238	0.277	0.317	0.357	0.397	0
10	0.397	0.437	0.477	0.517	0.557	0.597	0.637	0.677	0.718	0.758	0.798	10
20	0.798	0.838	0.879	0.919	0.960	1.000	1.041	1.081	1.122	1.163	1.203	20
30	1.203	1.244	1.285	1.326	1.366	1.407	1.448	1.489	1.530	1.571	1.612	30
40	1.612	1.653	1.694	1.735	1.776	1.817	1.858	1.899	1.941	1.982	2.023	40
50	2.023	2.064	2.106	2.147	2.188	2.230	2.271	2.312	2.354	2.395	2.436	50
60	2.436	2.478	2.519	2.561	2.602	2.644	2.685	2.727	2.768	2.810	2.851	60
70	2.851	2.893	2.934	2.976	3.017	3.059	3.100	3.142	3.184	3.225	3.267	70
80	3.267	3.308	3.350	3.391	3.433	3.474	3.516	3.557	3.599	3.640	3.682	80
90	3.682	3.723	3.765	3.806	3.848	3.889	3.931	3.972	4.013	4.055	4.096	90
100	4.096	4.138	4.179	4.220	4.262	4.303	4.344	4.385	4.427	4.468	4.509	100
110	4.509	4.550	4.591	4.633	4.674	4.715	4.756	4.797	4.838	4.879	4.920	110
120	4.920	4.961	5.002	5.043	5.084	5.124	5.165	5.206	5.247	5.288	5.328	120
130	5.328	5.369	5.410	5.450	5.491	5.532	5.572	5.613	5.653	5.694	5.735	130
140	5.735	5.775	5.815	5.856	5.896	5.937	5.977	6.017	6.058	6.098	6.138	140
150	6.138	6.179	6.219	6.259	6.299	6.339	6.380	6.420	6.460	6.500	6.540	150
160	6.540	6.580	6.620	6.660	6.701	6.741	6.781	6.821	6.861	6.901	6.941	160
170	6.941	6.981	7.021	7.060	7.100	7.140	7.180	7.220	7.260	7.300	7.340	170
180	7.340	7.380	7.420	7.460	7.500	7.540	7.579	7.619	7.659	7.699	7.739	180
190	7.739	7.779	7.819	7.859	7.899	7.939	7.979	8.019	8.059	8.099	8.138	190
200	8.138	8.178	8.218	8.258	8.298	8.338	8.378	8.418	8.458	8.499	8.539	200
210	8.539	8.579	8.619	8.659	8.699	8.739	8.779	8.819	8.860	8.900	8.940	210
220	8.940	8.980	9.020	9.061	9.101	9.141	9.181	9.222	9.262	9.302	9.343	220
230	9.343	9.383	9.423	9.464	9.504	9.545	9.585	9.626	9.666	9.707	9.747	230
240	9.747	9.788	9.828	9.869	9.909	9.950	9.991	10.031	10.072	10.113	10.153	240
250	10.153	10.194	10.235	10.276	10.316	10.357	10.398	10.439	10.480	10.520	10.561	250
260	10.561	10.602	10.643	10.684	10.725	10.766	10.807	10.848	10.889	10.930	10.971	260
270	10.971	11.012	11.053	11.094	11.135	11.176	11.217	11.259	11.300	11.341	11.382	270
280	11.382	11.423	11.465	11.506	11.547	11.588	11.630	11.671	11.712	11.753	11.795	280
290	11.795	11.836	11.877	11.919	11.960	12.001	12.043	12.084	12.126	12.167	12.209	290
300	12.209	12.250	12.291	12.333	12.374	12.416	12.457	12.499	12.540	12.582	12.624	300
310	12.624	12.665	12.707	12.748	12.790	12.831	12.873	12.915	12.956	12.998	13.040	310
320	13.040	13.081	13.123	13.165	13.206	13.248	13.290	13.331	13.373	13.415	13.457	320
330	13.457	13.498	13.540	13.582	13.624	13.665	13.707	13.749	13.791	13.833	13.874	330
340	13.874	13.916	13.958	14.000	14.042	14.084	14.126	14.167	14.209	14.251	14.293	340
°C	0	1	2	3	4	5	6	7	8	9	10	°C

Appendix B

Table 3. Analyzed average monthly sunshine hours of Jimma for five years

year	Jan	Feb	Mar	Apr	May	Jun	Jul	Aug	Sep	Oct	Nov	Dec
2013	8.69	8.76	7.01	7.49	5.59	5.17	2.73	3.56	5.11	6.74	7.7	8.18
2014	6.83	6.67	7.15	7.24	6.9	6.19	3.27	4.07	5.14	6.41	7.41	7.81
2015	8.09	8.14	7.97	7.8	6.53	4.31	4.9	4.59	6.4	8.4	7.2	6.51
2016	6.92	7.46	7.29	5.02	5.4	4.65	3.06	4.49	5.75	8.19	7.9	8.54
2017	8.78	7.33	7.75	7.99	5.93	5.97	3.13	3.86	5.15	6.41	7.55	8.38
Av.shr	7.86	7.67	7.43	7.11	6.07	5.26	3.42	4.12	5.51	7.23	7.55	7.89

Table 4. Five year analyzed solar radiations of Jimma

Month	n_d	$\delta(°)$	$\omega_s(°)$	N (hrs)	n (hrs)	$\frac{n}{N}$	a	b	H_o(kwh/ m2/d)	H (kwh/ m2/d)
January	17	-20.9	87.05	11.61	7.86	0.68	0.3	0.43	9.48	5.61
February	47	-13.0	88.22	11.76	7.67	0.65	0.29	0.44	9.83	5.67
March	75	-2.4	89.67	11.96	7.43	0.62	0.28	0.45	10.38	5.83
April	105	9.4	91.27	12.17	7.10	0.58	0.27	0.47	9.88	5.34
May	135	18.8	92.62	12.35	6.07	0.49	0.24	0.5	9.91	4.84
June	162	23.1	93.29	12.44	5.23	0.42	0.22	0.52	9.23	4.09
July	198	21.2	92.99	12.4	3.42	0.28	0.18	0.57	9.92	3.41
August	228	13.5	91.85	12.25	4.12	0.34	0.2	0.55	10.15	3.94
September	258	2.2	90.29	12.04	5.51	0.46	0.24	0.51	10	4.69
October	288	-9.6	88.69	11.83	7.23	0.61	0.28	0.46	10.28	5.72
November	318	-18.9	87.35	11.65	7.55	0.65	0.29	0.44	10.05	5.8
December	344	-23.0	86.72	11.56	7.88	0.68	0.3	0.43	9.81	5.8
Annual average							0.26	0.48	9.91	5.06

Appendix C

Questionnaire form

This questionnaire is prepared for academic study purpose and you are kindly asked to give your answers. Fill the box with the sign X in the space provided.

Address_____

1. Number of residents in the house? _____
2. What is the main source of energy for cooking?
   Wood/biomass ☐   electricity ☐   coal ☐   kerosene ☐   other _____
3. How much per week do you spend for cooking in birr
   Up to 50 ☐   51-100 ☐   100-150 ☐   above 150 ☐
4. How much water do you add for lunch or dinner per cooking vessel

   Lunch   dinner

   0 to 0.5 litter ☐   0 to 0.5 litter ☐

   0.5 - 1 litter   ☐   0.5 - 1 litter   ☐

   1 - 1.5 litter   ☐   1 - 1.5 litter   ☐

   1.5 – 2 litter   ☐   1.5 – 2 litter   ☐

   Above 2 litter   ☐   Above 2 litter   ☐

5. What stew do you commonly use?
   Lunch   Dinner
   Shiro ☐   shiro ☐
   Lentils ☐   lentils ☐
   Gomen ☐   gomen ☐
   Potato ☐   potato ☐
   Rice   ☐   rice   ☐
   Meat   ☐   meat   ☐
   Macaroni/spaghetti ☐   Macaroni/spaghetti ☐
   If other specify _____   if other specify _____
6. When using wood biomass what do you think the main problem is?
   Smoke ☐   Supply ☐   Cost ☐   Labor ☐   If other specify_____
7. By using electricity, which part do you think prevail, pros/cons?
   Pros ☐   why? _____
   Cons ☐   why? _____
8. Do you know solar energy can be used as a source for cooking?
   Yes ☐   no ☐
9. If there is solar cooker do you want to buy it?
   Yes ☐   no ☐

Thank you very much for your cooperation!!!

71